Electromagnetic Cell Level Calibration for ATLAS Tile Calorimeter Modules

Y.A.Kulchitsky[1], **P.V.Tsiareshka**
Academy of Sciences of Belarus, Institute of Physics, Minsk, Belarus
& Joint Institute for Nuclear Research, Dubna, Russia

J.A.Budagov, J.I.Khubua[2],
N.A.Rusakovich, V.B.Vinogradov
Joint Institute for Nuclear Research, Dubna, Russia

A.M.Henriques
CERN, Geneva, Switzerland

T.Davidek
Charles University in Prague, Prague, Czech Republic

S.Tokar
Comenius University, Bratislava, Slovakia

A.Solodkov
Institute for High Energy Physics, Protvino, Russia

I.Vichou
University of Illinois, Urbana – Champaign, Illinois, USA

[1]Corresponding author; e-mail: Iouri.Koultchitski@cern.ch
[2]Also HEPI, Tbilisi State University, Tbilisi, Georgia

Abstract

We have determined the electromagnetic calibration constants of 11% TileCal modules exposed to electron beams with incident angles of 20° and 90°. The gain of all the calorimeter cells have been pre-equalized using the radioactive Cs-source that will be also used in situ. The average values for these modules are equal to: for the flat filter method 1.154±0.002 pC/GeV and 1.192±0.002 pC/GeV for 20° and 90°, for the fit method 1.040±0.002 pC/GeV and 1.068±0.003 pC/GeV, respectively. These average values for all cells of calibrated modules agree with the weighted average calibration constants for separate modules within the errors. Using the individual calibration constants for every module the RMS spread value of constants will be 1.9±0.1%. In the case of the global constant this value will be 2.6±0.1%. Finally, we present the global constants which should be used for the electromagnetic calibration of the ATLAS Tile hadronic calorimeter data in the ATHENA framework. These constants are equal to 1.15 pC/GeV in the case of the flat filter method and 1.04 pC/GeV for the fit one.

1 Introduction

The constructed ATLAS detector at the LHC will have the huge physics discovery potential, in particular in the detection of a heavy Higgs boson [1, 2]. Calorimeters will play a crucial role in it. The key question of calorimetry is the absolute energy calibration, in particular the calibration in the electromagnetic energy scale.

The physics goals have led to the following requirement for the knowledge of the absolute scale of energy: in the case of hadronic jets, the scale should be known to an accuracy of 1% [3].

The other important issue is the energy linearity. The most stringent linearity requirements for the hadronic calorimeter come from the study of quark compositeness where the jet energy scale has to be linear within 1.5% up to the transverse energy of 4 TeV [2, 4].

For each cell of the ATLAS hadronic TileCal calorimeter [5] the calibration constants, which define the relationship between the calorimeter signals, expressed in picoCoulombs, and the energy of the absorbed particles, which produced the signals, must be determined. The calibration constants depend on the type of particle, or jet and, generally speaking, on their energies [6]. This means that calibration constants determined for one particular type of particle, or jet of one particular energy lead to systematic mis-measurements of energy if used for the interpretation of signals caused by other particles, or jets of other energies.

It is assumed that for the ATLAS calorimeters the hadronic final states physics objects (hadrons, jets, missing transverse energy) should be reconstructed at first using calorimeter signals on an electromagnetic energy scale [7, 8].

With the aim of establishing of this scale and understanding of performance of the ATLAS Tile hadronic calorimeter [5] to electrons 11% of modules have been exposed in electron beams with various energies by three possible ways: cell-scan at $\theta = 20^\circ$ at the centers of the front face cells, η-scan and tilerow scan at $\theta = 90^\circ$ for the module side cells.

Our work is devoted to summary of the electromagnetic calibration constants of TileCal modules at 20° and 90° obtained by us and presented in the following talks and notes [9] – [20].

The obtained calibration constants have been included in the TileCal calibration database and will be used for the energy calibration of the ATLAS Tile hadronic calorimeter.

Besides our works there are ones in which the electromagnetic calibration constants of TileCal modules at 20° and 90° for some testbeam runs have been determined [21] – [25].

2 The ATLAS Hadron Tile Calorimeter

The ATLAS Hadron Tile Calorimeter (TileCal) is a 2900 t sampling calorimeter using iron as passive material and tiles of scintillator as active material readout by wavelength shifting fibers [5]. This calorimeter will play a very important role to identify jets, measure their energy and direction, reconstruct the transverse missing energy. The goal of the TileCal is to measure hadrons energy with good resolution ($\sigma/E = 50\%\sqrt{GeV}/\sqrt{E} \oplus 3\%$) and linearity (1 – 2% up to TeV scale).

An innovative feature of this calorimeter is the orientation of the scintillators that are placed in planes perpendicular to the colliding beams (Fig. 1 (left)). This disposition simplifies the tile-fiber and fiber-PMT coupling reducing the dead spaces of the calorimeter and hence increasing hermecity. Due to this feature we can get an hermetic coverage up to $\mid \eta \mid = 1.7$ ($\mid \eta \mid = 5$ with forward calorimeters), very important for the reconstruction of the transverse missing energy.

The TileCal is divided into one barrel and two extended barrel sections. All three sections have a cylindrical structure with an inner radius of 2280 mm and outer one of 4230 mm. The barrel section is 5460 mm in length along the beam axis, while each extended barrel has a length of about 2910 mm. Each of the cylinders is further subdivided into 64 independent azimuthally oriented modules. Within each module, there are a number of readout cells. Each cell is a set of scintillating tiles connected by fibers to 2 PMTs. The TileCal will contain 4672 cells which will be read-out by 9344 PMTs. Two fibres collect light from every scintillator tile at both of its azimuthal edges. The total number of tiles is 456000.

The calorimeter is divided in η towers, which are "pseudo-projective" towards the interaction region, and radially segmented in three depths. The thicknesses of depths at $\eta = 0$ are 1.5 λ in the first sampling, 4.2 λ in the second one, and 1.9 λ in the third one, with a total depth of 7.6 λ. The granularity $\Delta\eta \times \Delta\varphi$ at $\eta = 0$ is 0.1×0.1 for the first two depths and 0.2×0.1 in the third compartment.

The iron structure of each module consists of a number of repeated periods (Fig. 1 (right)). Each period is 18 mm thick and consists of four

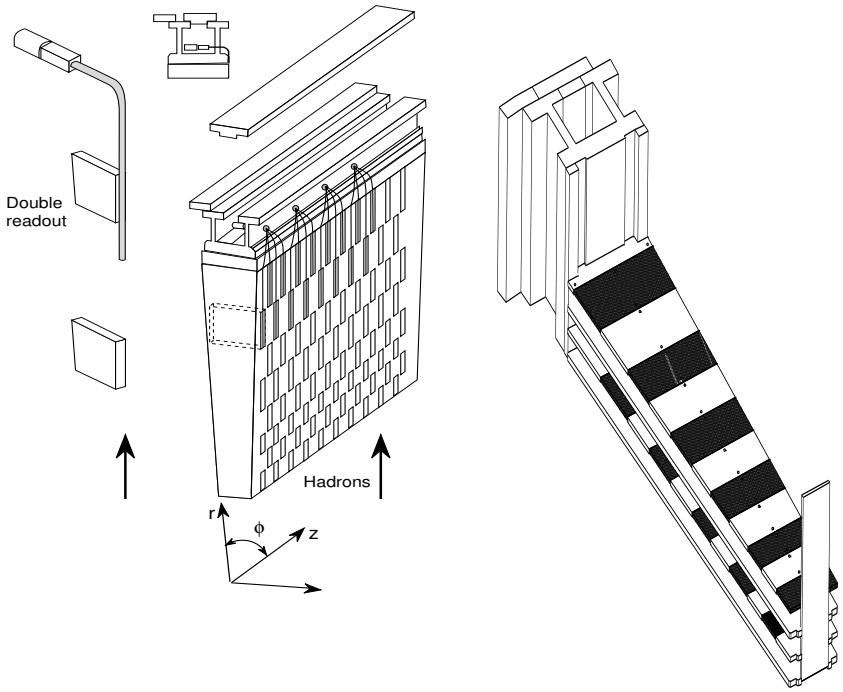

Figure 1: Principle of the TileCal (left). Exploded view of an assembled TileCal period (right).

layers. The first and third layers are formed by large trapezoidal steel plates (master plates), and spanning the full longitudinal dimension of the module. In the second and fourth layers, smaller trapezoidal steel plates (spacer plates) and scintillator tiles alternate. These layers consist of 11 different trapezoids of steel and scintillator, each spanning from 97 to 187 mm. The master plates, spacer plates and scintillator tiles are of 5 mm, 4 mm and 3 mm thick, respectively. The iron to scintillator ratio is 4.67:1 by volume.

3 Test Beam Setup

Fig. 2 shows the used test beam setup. The Barrel Module 0 is the bottom module mounted on the table. The middle layer is the production barrel module BM. The top layer is the two extended barrel modules: EBM+ for $\eta > 0$ (beam left) and EBM− for $\eta < 0$ (beam right).

The layout of the cell geometry is demonstrated in Fig. 3. Each cell

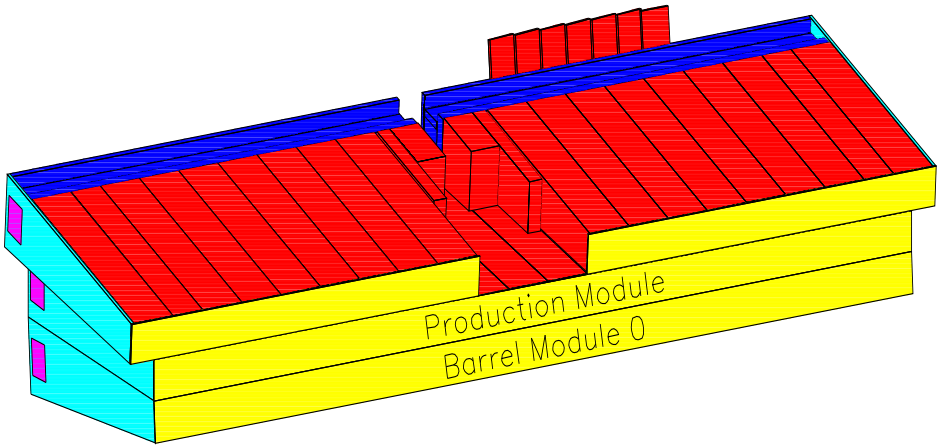

Figure 2: Sketch of the test beam setup.

is a set of scintillating tiles connected by fibers to 2 PMTs. Each module is read out in three longitudinal layers. The first layer consists of A-cells, the second one — of B- and C-cells, and the third one — of D-cells. In η, the readout cells, built by grouping fibres into PMTs, are "pseudo-projective" towards the interaction region. There are 11 transverse rows of tiles (tilerows) in a module. For a barrel module A-cells have tilerows 1÷3, B- and C-cells — 4÷7, D-cells — 8÷11. For a extended barrel module A-cells have tilerows 1÷3, B- and C-cells — 4÷7, D-cells — 8÷11.

4 PMT signal reconstruction methods

For obtaining of the channel response the registered PMT signals are treated by two methods: the flat filter and fit ones [26, 27]. The response of the flat filter method, R_{flat}, is an integral, a maximum of all possible sums of 5 subsequent samples of the pulse shape of a PMT signal which is sampled 9 times with the 25 ns interval

$$R_{flat} = C_{cis} \cdot \max \left(\sum_{i=j}^{j+4} (s_i - s_1) \right). \qquad (1)$$

The first sample (s_1) is considered as a pedestal and its value is subtracted from all other samples (s_i). Here C_{cis} is the constant transforming the

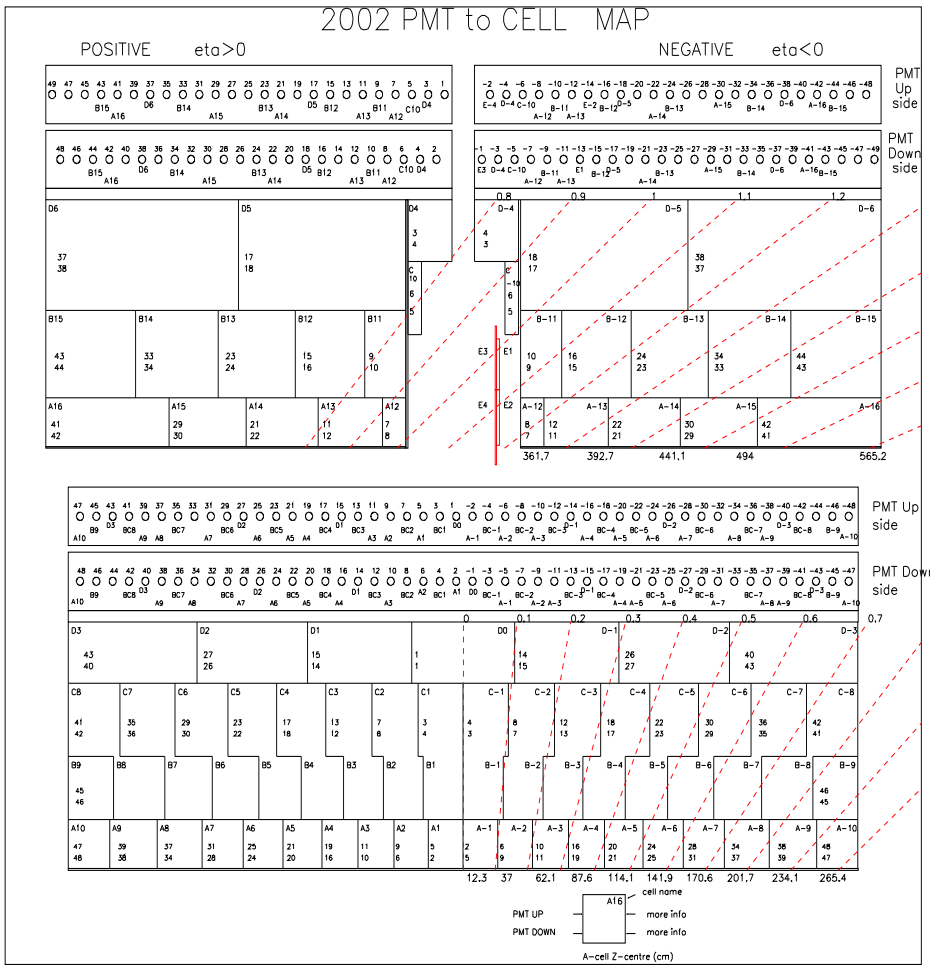

Figure 3: The layout of the cell geometry.

ADC values into pC derived from CIS (Charge Injection System) events, $j = 1, \ldots, 5$. As a consequence of finding the maximum, the flat filter method exhibits positive offset for the pedestal-like events. For majority of PMTs this offset, $\langle R_{noise} \rangle$, and RMS_{noise} do not exceed 0.016 pC and 0.06 pC, correspondingly, amounts to 0.01 pC and 0.05 pC, in average, as can be seen in Fig. 4. But there are tails, 11% PMTs are with larger noise. Because of this, at using the method of cutting noise (in which the PMT channel signal is set equal to 0 if the value of signal less than Cut_{noise} value, with a typical value of 0.1 pC) the calibration constants at low energies (10 – 20 GeV) become dependent from a value of Cut_{noise}

as shown in Fig. 4 (bottom). The data at high energy are insensitive to the value of Cut_{noise}, as expected.

We have devised the following algorithm correcting this defect. If the value of signal less than $3 \cdot RMS_{noise,i}$ then the one is decreased on the value of $\langle R_{noise,i} \rangle$. So, we obtain unbias values of $\langle R_{noise,i} \rangle$.

The fit method is based on fitting the pulse shape function, f (t), to samples (s_i) of event

$$f(t) = R_{fit} \cdot g(t - \tau) + ped, \tag{2}$$

where $g(t-\tau)$ is the known normalized pulse shape function, t is time, τ is the phase (peak position in time), *ped* is a pedestal. So, the reconstructed response, R_{fit}, is the amplitude of the PMT signal. The fit method results only in a very small offset (typical values are 0.0002 pC per PMT) and smaller spread, $\langle RMS_{noise,i} \rangle$ is 0.02 pC.

5 Data analysis

5.1 Calibration volume

The area used for reconstructing the electron energy for both the 20° and 90° runs, was one TileCal extended barrel module or half barrel module, since the electron calibration constants are used for the hadron energy reconstruction [28, 29]. These calorimeter volumes have a number of cells similar to the amount of cells that we use to reconstruct an hadronic shower [30]. Given the fact that the electron beam was incident in the center of each cell for 20° runs or of the each tile row for 90° runs, there was no lateral leakage due to the fact that one module was used for the energy estimation. Even though a larger area than the shower extent was used, the volume that was used for electron energy reconstruction was that of one cell, since more than 90% of the electron shower is contained in one cell. Each cell contributes with about 30 MeV of electronics noise (fit method), having no impact on the calibration constants. The cells calibrated, due to the electromagnetic shower longitudinal size, are the A-layer cells (20° beams) and the cells on the Z-edge of the modules (90° beams) for each module, representing approximately 50% of the module's readout cells.

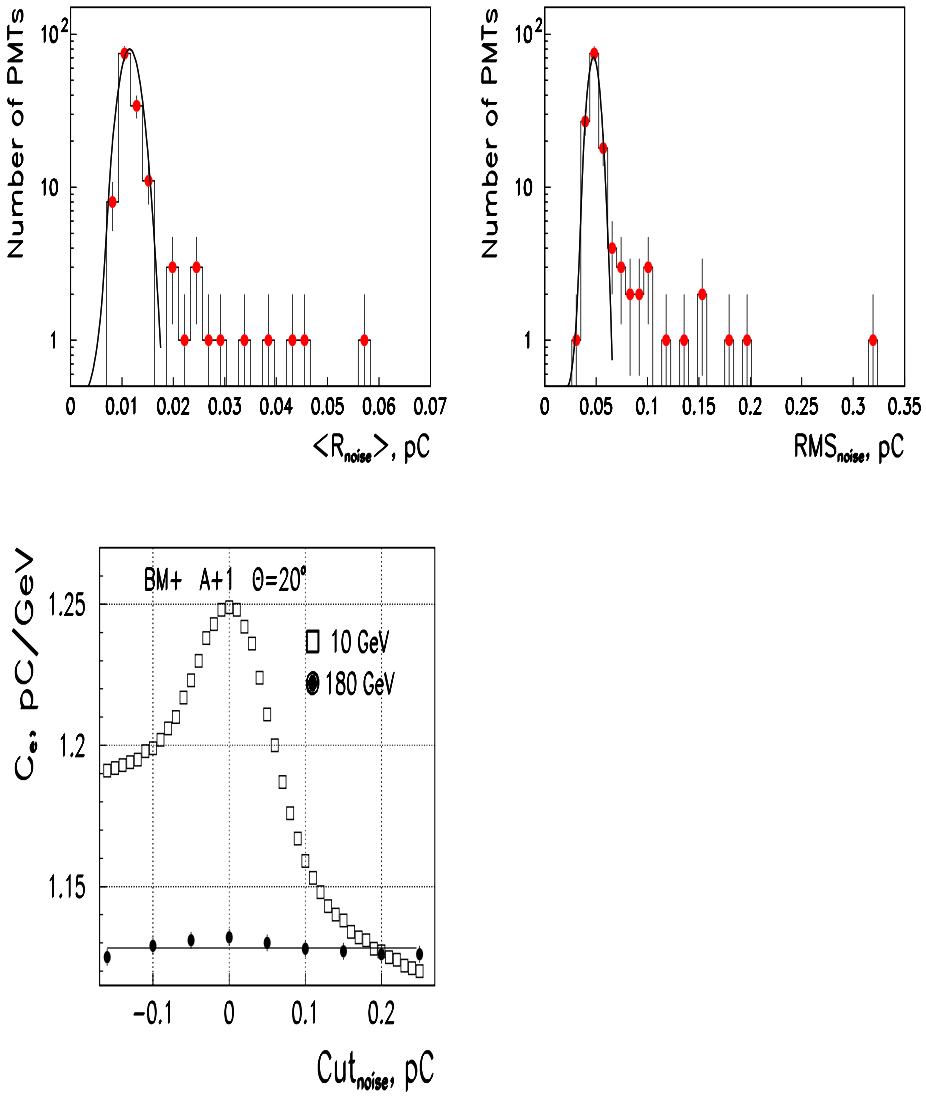

Figure 4: The distributions of mean values of PMT noise (top left) and RMS values (top right) of PMTs used in the test beam July 2002 (JINR-55, ANL-44, IFA-42). The electron calibration constants, C_e, for the A+1 cell of BM+ (JINR-55) at $\theta = 20°$ for 10 and 180 GeV as a function of Cut_{noise} value (bottom).

5.2 Electron selection

The H8 electron beams at the SPS CERN are the mixture of electrons, muons and hadrons. For calibration it is important to have the pure electron beam. We have estimated that in order to have the systematic error in the electron calibration constant due to the pion contamination smaller than 0.3% this contamination must be smaller than 1.5% in the energy range of 10 – 300 GeV [31]. Therefore, we have performed the identification of (e, μ, π) particles on the basis of the calorimetric information. We have used the following three selection criteria [31].

5.2.1 Selection with longitudinal shower energy deposition

The first selection criterion

$$C_i = \sum_{selected\ i} \sum_{k=1}^{2} \sum_{l=1}^{2} E_{ikl}/E_{beam}, \tag{3}$$

is a value of the relative shower energy deposition in the first two calorimeter depths, where E_{ikl} is the energy response of an ikl PMT, $[E_{ikl}] = \text{pC}$, k is a depth number, i is a cell number in the k-depth, $l = 1,\ 2$ is the PMT number in the ik cell, $[C_i] = \text{pC/GeV}$.

The basis for this electron-hadron separation is the different longitudinal energy deposition for electrons and hadrons. For example, if a 100 GeV particle crosses 45 cm of the Tile calorimeter from the front face it corresponds to 18 radiation lengths or 2.2 nuclear interaction lengths. The amount of the deposited energy is equal to 95% for the electromagnetic shower and only 50% for the hadronic shower [32].

Fig. 5 (left) shows the typical C_i distributions. The left peak corresponds to the pion events, the right peak corresponds to the electron events.

5.2.2 Selection using lateral shower energy deposition

The second selection criterion is related with the lateral shower spread

$$E_{cut} = \frac{\sqrt{\sum_c (E_c^\alpha - \sum_c E_c^\alpha / N_{cell})^2}}{\sum_c E_c^\alpha}\ , \tag{4}$$

where $1 \le c \le N_{cell}$, N_{cell} is the used cells number, $\alpha = 0.6$. For example, for the 100 GeV hadronic shower the 99% containment radius is equal to 430 mm, but for the electromagnetic shower the one is equal to 70 mm.

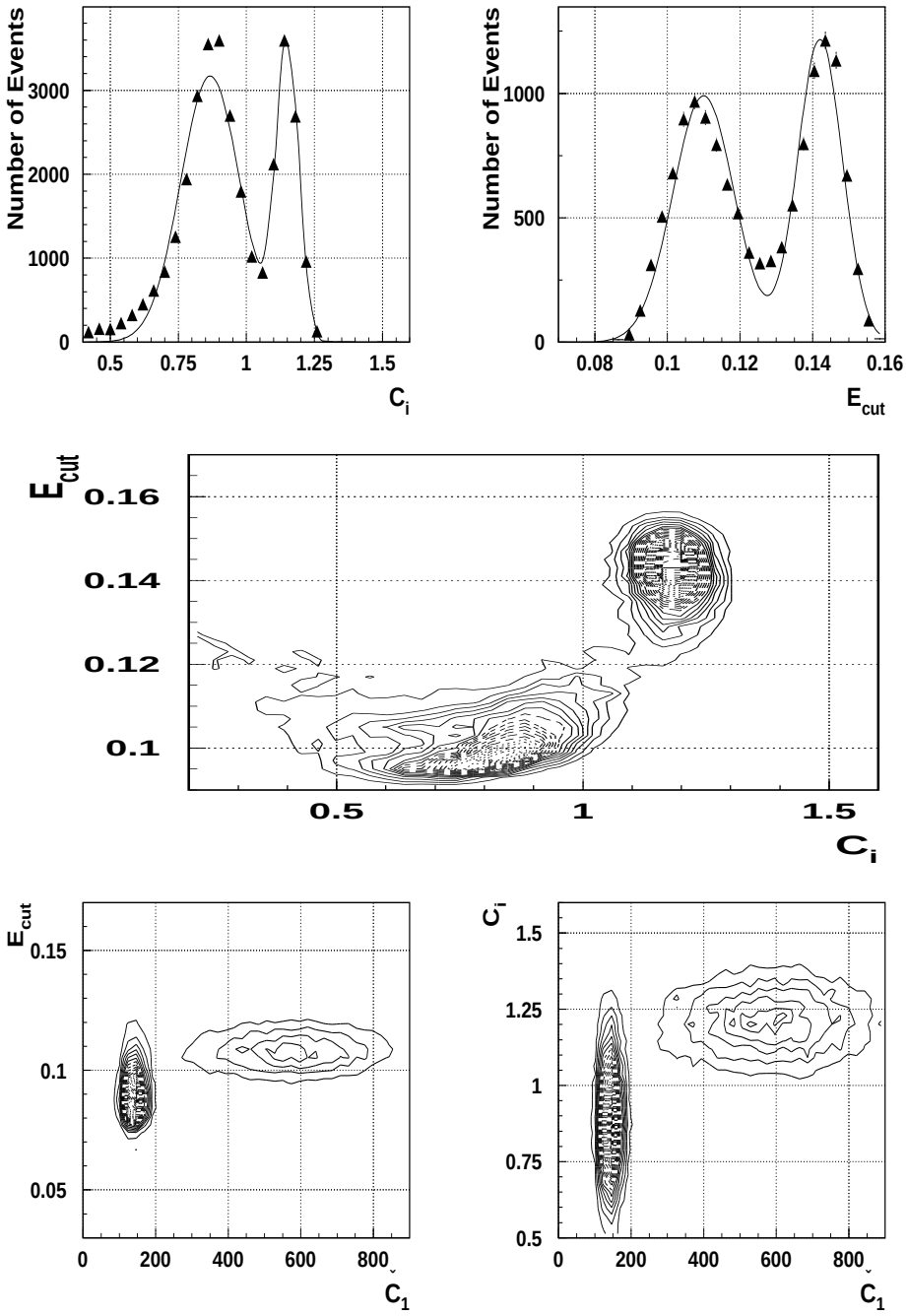

Figure 5: The C_i (top-left) and E_{cut} (top-right) distributions and the scatter plot E_{cut} versus C_i (middle). The scatter plots of E_{cut} vs $\check{\mathrm{C}}_1$ and C_i vs $\check{\mathrm{C}}_1$ (bottom).

Fig. 5 (center) shows the typical E_{cut} distributions. The left peak corresponds to the pion events, the right peak corresponds to the electron events. Fig. 5 (right) shows the scatter plot of E_{cut} versus C_i. The top right region are the electron events, the bottom left region are the pion events. These Figures allow to determine the values of the cuts and to estimate the contaminations.

We have estimated by extrapolation of the fitted pion peak curve to the region of the electron peak (Figs. 5) that the contamination of the pion events in the electron events does not exceed the 0.2% level [31].

5.2.3 Rejection of muons

For the muon rejection at energies $E_{beam} \geq 10$ GeV we have used the cut in the total deposited energy: $E_{tot} > E_{min}$ with $E_{min} = 5$ GeV [33]. This cut effectively selects muons as muons loose a very small fraction of their energy in the calorimeter.

5.2.4 Electrons selection using Cherenkov counter

At energies ≤ 20 GeV there is a bad selection of electrons by the C_i and E_{cut} criteria. This situation is greatly improved by using the first Cherenkov counter signal (cut 3).

Fig. 5 (bottom) shows the typical scatter plots of E_{cut} versus $\check{\mathrm{C}}_1$ and C_i versus $\check{\mathrm{C}}_1$. As seen, electrons (left) are well selected.

5.2.5 Resultant cuts

We have used the following three cuts for the electron selection [31]: the cut 1 is $C_i > 0.9 \div 1.1$, the cut 2 is $E_{cut} > 0.07 \div 0.14$, the cut 3 is $\check{\mathrm{C}}_1 > 200 \div 400$.

Due to these cuts we have obtained the clean sample of the electron events for the calibration of modules of the TileCal.

5.3 Tilecal electron response

The electron response in our calorimeter is a function of a beam energy, and an incidence angle, and an impact point [34].

The energy response spectrum for given run (beam has the transversal spread ± 15 mm) as a rule is non-Gaussian as can be seen in Fig. 6.

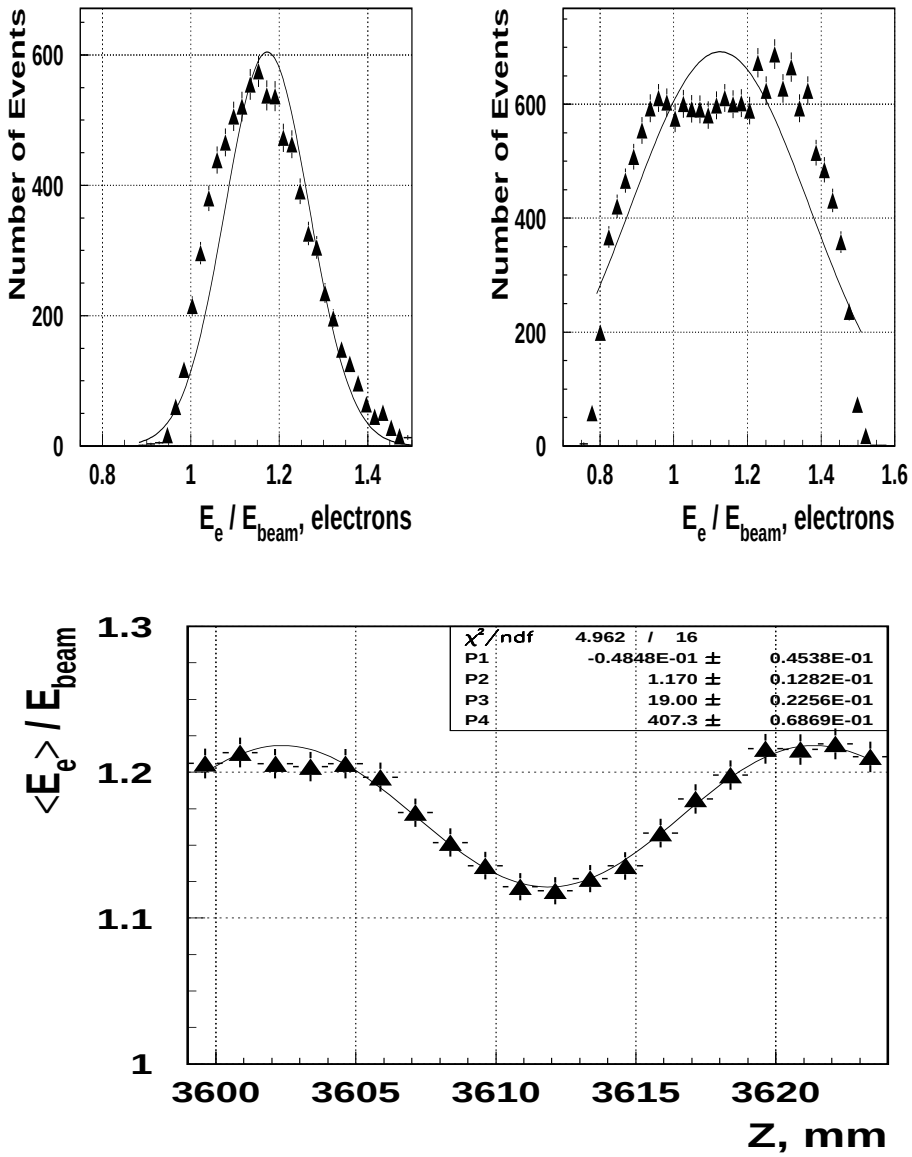

Figure 6: The relative electron energy distributions (pC/GeV for $E = 10$ GeV at $\theta = 20°$ (top-left) and for $E = 20$ GeV at $\eta = -0.15$ (top-right). The normalized electron response (E_e/E_{beam}) for $E = 20$ GeV as a function of impact point Z coordinate (bottom).

The mean normalized electron responses as a function of an impact point Z coordinate for A-cells and η scans are described by the sine function (Fig. 6, bottom):

$$f(Z) = P_2 + P_1 \sin(2\pi Z/P_3 + P_4) \tag{5}$$

5.4 Test beam periods

Table 1 gives the realized Test Beam runs, exposed TileCal modules and references of our analysis.

Table 1: Test Beam runs, Exposed TileCal modules, references of our analysis, Figures and Tables, relevant to given Test Beam run.

$N^{\underline{o}}$	TB	Modules			Runs	Analysis	Figs	Tables
		Extended Barrel		Barrel	available			
1	08-2001	ANL-15	IFA-38	JINR-18	Flat	[9]		
2	09-2001		IFA-15 IFA-24		Flat	[10]	19	8, 9
3	06-2002	ANL-08	IFA-59	JINR-34	Flat	[11]	20–25	10–15
4	07-2002	ANL-44	IFA-42	JINR-55	Flat, Fit	[12, 13]	26–29	16–35
5	08-2002	ANL-27	IFA-09	JINR-01	Flat	[14]	30	36–41
6	06-2003	ANL-03 ANL-23		JINR-12	Flat, Fit	[15]	31–33	42–47
7	07-1-2003	ANL-30	IFA-27	JINR-27	Flat, Fit	[16, 17]	34–36	48–58
8	07-2-2003	ANL-36	IFA-46	JINR-54	Flat, Fit			
9	08-2003			JINR-13 JINR-63	Flat, Fit	[24, 25]		

Figs. 19 – 36 in Appendix B show the obtained calibration constants for various testbeam periods 2 – 7 presented in the Table 1.

The numerical values of these constants are given in Tables 8 – 58 and presented in the Appendix C.

The correspondence between production ANL, IFA, JINR modules number and position of these EBA, EBC, LB modules in the assembled TileCal presented in the Appendix D in the Table 59.

6 Electromagnetic calibration of TileCal

The summary of the numerical values of the average electromagnetic calibration constants and RMS of TileCal 19 modules (ANL-03, ANL-08, ANL-23, ANL-27, ANL-30, ANL-44, IFA-09, IFA-15, IFA-24, IFA-27, IFA-42, IFA-9, JINR-01, JINR-12, JINR-13, JINR-27, JINR-34, JINR-55, JINR-63) is given in the Tables 6 and 7 in Appendix A.

For 90° runs, the results are presented both with the default Cs calibration (Default) and also with the individual tilerow corrections (Corrected). In the former case a Cs correction factor averaging the responses of all tile rows in a cell is applied, whereas in the latter each tile row response is corrected by its individual Cs correction factor. The difference is further discussed in Section 7.

All the modules (11%) have been analysed with flat filter method. For historical reasons only a part of modules have also been analysed with the fit method (in 2002, 2003). In addition, all this analysis is performed without ANL-03 module in cell-scan (Test beam June 2003) due to problems in Cs-calibration in this particular case.

Let us first compare the performance with two above mentioned energy reconstruction methods with the same modules, therefore at limited statistics (see Section 6.1). Next, the full statistics results are presented for the flat filter (see Section 6.2). The overall Tile calorimeter performance with electrons in terms of the uniformity and the response angular dependence is then discussed in Sections 7 and 7.3.

6.1 Comparison of the Flat and Fit methods results

As already mentioned above, results presented in this Section involve only 3 testbeam periods (TB-07-2002, TB-06-2003 and first part of TB-07-2003), where both flat filter and fit method analysis were performed. Thus, these results represent limited statistics. Fig. 7 and Table 2 present the average and RMS values for the electromagnetic calibration constants with two reconstruction methods (the flat filter and the fit methods) using the July 2002, June 2003 and fist period of July 2003 test beam data for all modules at 20° with the default Cesium calibration and with the individual tilerow correction at 90° using the Cesium calibration system (see Section 7.1 for more details). The same results for separate type of modules ANL, IFA, JINR are presented in the Table 3.

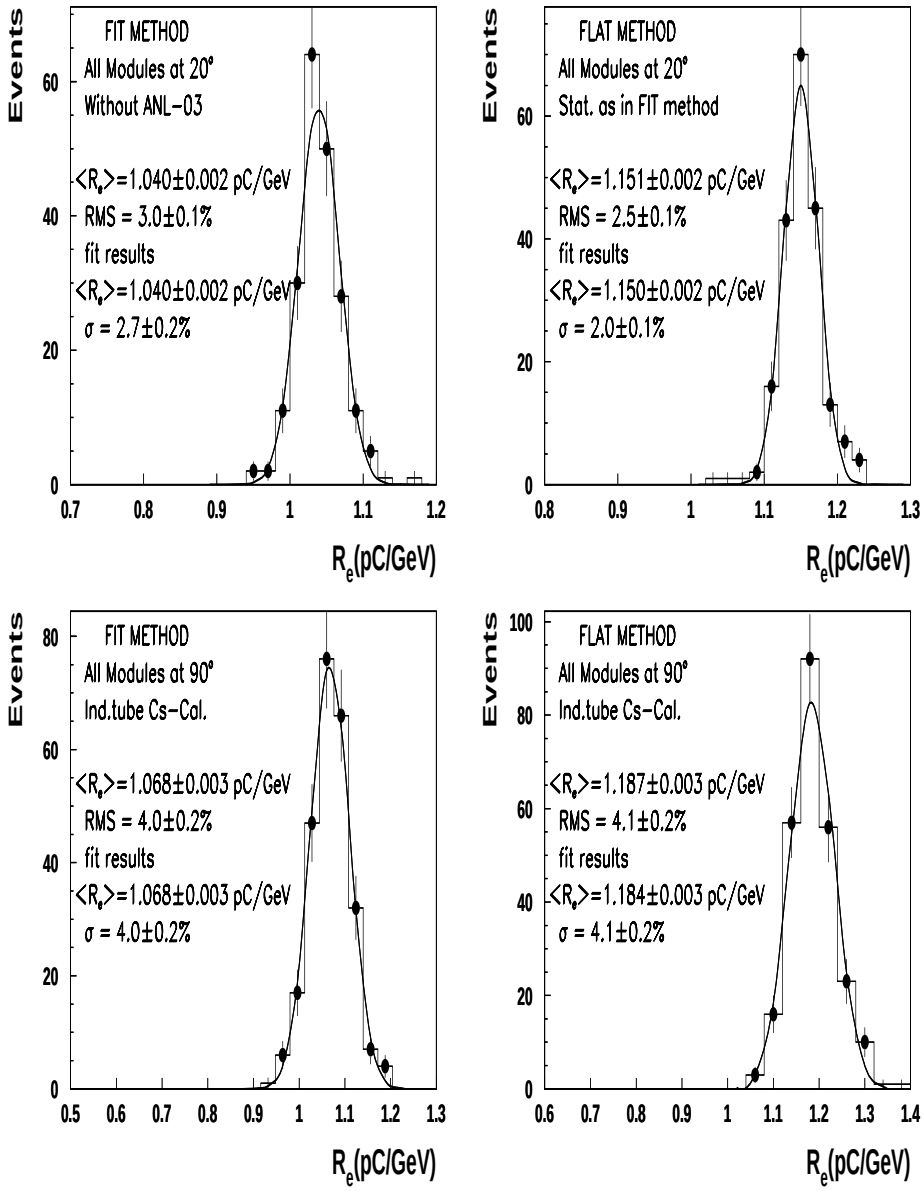

Figure 7: The distributions of electromagnetic calibration constants electrons at $\theta = 20°$ (top) and at $\theta = 90°$ (bottom) for all modules: for the fit method (left) and the flat filter method (right) at the limited statistics.

Table 2: The average and the RMS values of the electromagnetic calibration constants for two reconstruction methods (the flat filter and fit methods) using the TB-07-2002, TB-06-2003 and the first period of TB-07-2003 test beam data for all Modules at 20° with the default Cesium calibration and at 90° with the individual tilerow correction at 90° using the Cesium calibration system.

Θ	Flat Method		Fit Method		Flat/Fit
	$\langle R_e \rangle$ pC/GeV	RMS %	$\langle R_e \rangle$ pC/GeV	RMS %	$\frac{\langle R_e \rangle_{Flat}}{\langle R_e \rangle_{Fit}}$
20°	1.151±0.002	2.5±0.1	1.040±0.002	3.0±0.2	1.107±0.003
90°	1.187±0.003	4.1±0.2	1.068±0.003	4.0±0.2	1.111±0.004
90°/20°	1.031±0.003		1.027±0.003		

Table 3: The average and the RMS values of the electromagnetic calibration constants for two reconstruction methods (the flat filter and fit methods) using the TB-07-2002, TB-06-2003 and the first period of TB-07-2003 test beam data for ANL, IFA and JINR Modules at 20° with the default Cesium calibration and with the individual tilerow Cs correction at 90°.

		Flat Method		Fit Method		Flat/Fit
Θ	Module	$\langle R_e \rangle$ pC/GeV	RMS %	$\langle R_e \rangle$ pC/GeV	RMS %	$\frac{\langle R_e \rangle_{Flat}}{\langle R_e \rangle_{Fit}}$
20°	ANL	1.150 ±0.006	3.7±0.3	1.024 ±0.004	3.7±0.4	1.123 ±0.006
	IFA	1.147 ±0.003	2.6±0.2	1.041 ±0.004	2.0±0.2	1.102 ±0.005
	JINR	1.156 ±0.002	2.3±0.1	1.042 ±0.003	3.1±0.2	1.109 ±0.003
90°	ANL	1.182 ±0.007	3.9±0.4	1.052 ±0.005	3.7±0.4	1.124 ±0.007
	IFA	1.203 ±0.009	5.5±0.4	1.081 ±0.008	5.3±0.5	1.113 ±0.009
	JINR	1.183 ±0.004	3.2±0.2	1.071 ±0.004	3.3±0.2	1.105 ±0.005

The electron calibration constants for 20° and 90° obtained with the flat filter method are systematically higher than those obtained with the fit method by about 11%. This difference has no direct impact on the calorimeter performance once the respective factors are applied.

The calibration constants differ for 20° and 90° as also demonstrated in Table 2. This feature is further discussed in Section 7.3.

6.2 Results on the full statistics

In Section 6.1 we compared the results obtained with the flat filter and fit methods for a subset of the modules, where both analysis have been performed. The results presented in this section involve all modules exposed to particle beams, due to historical reasons (see Section 6.1) they are obtained with the flat filter only.

Figs. 8, 9 and Table 4 present the average and RMS values of the electromagnetic calibration constants with the flat filter reconstruction method using data from test beam periods TB-09-2001 – TB-07-1-2003 (see Table 1) for the ANL, IFA, JINR modules and all modules at 20° with the default Cesium calibration and with the individual tilerow Cs-correction at 90° (see Section 7.1 for more details).

Table 4: The average and RMS values of all electromagnetic calibration constants, extracted from Figs. 8 – 9, using the flat method for JINR, ANL, IFA and all modules at 20° (without ANL-03 module) and at 90°.

Module	20°		90°		90°/20°
	$\langle R_e \rangle$ pC/GeV	RMS %	$\langle R_e \rangle$ pC/GeV	RMS %	$\frac{\langle R_e \rangle_{90°}}{\langle R_e \rangle_{20°}}$
ANL	1.150 ±0.005	3.4±0.3	1.190 ±0.005	4.2±0.3	1.034 ±0.006
IFA	1.147 ±0.003	2.6±0.2	1.195 ±0.005	4.9±0.3	1.042 ±0.06
JINR	1.156 ±0.002	2.3±0.1	1.192 ±0.002	3.0±0.1	1.031 ±0.003
All	1.154 ±0.002	2.6±0.1	1.192 ±0.002	3.9±0.1	1.033 ±0.003

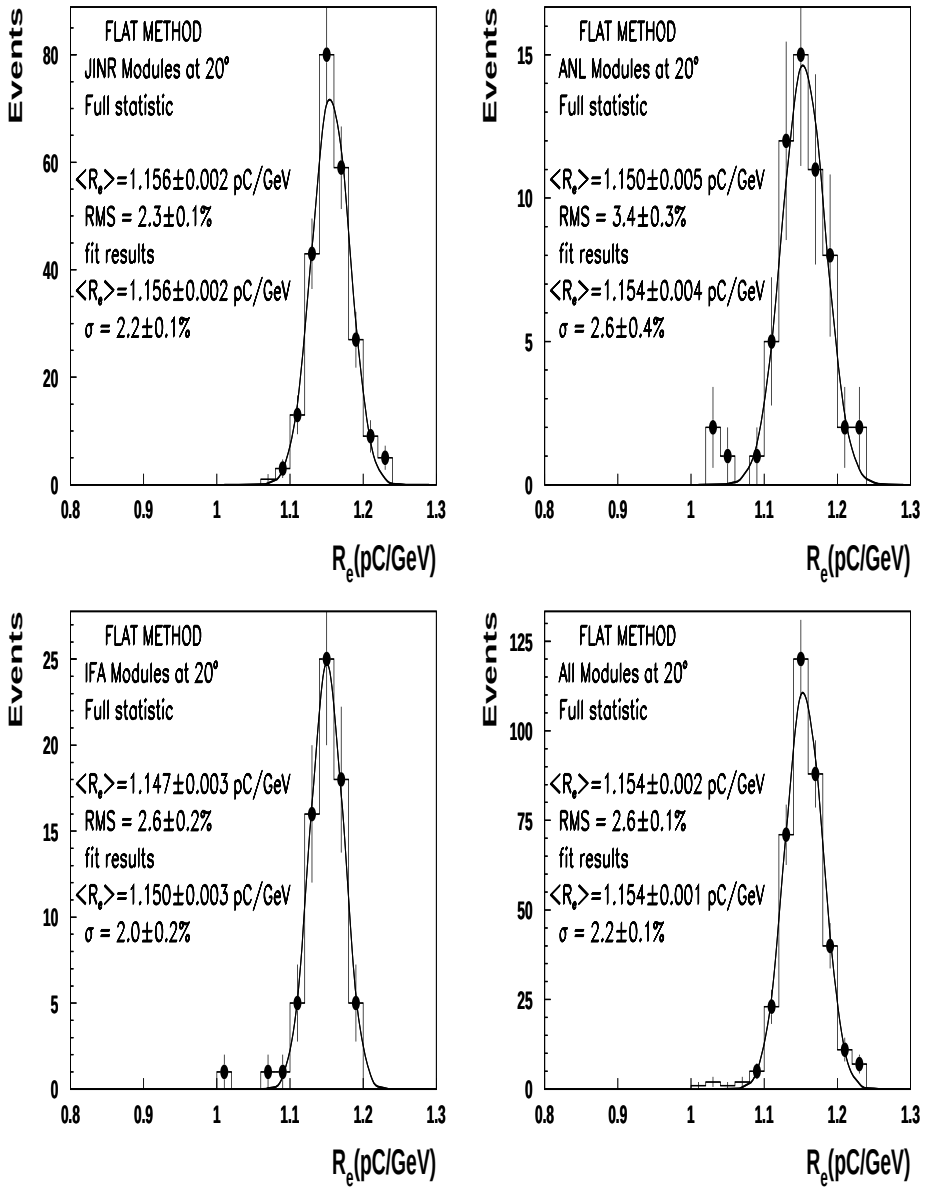

Figure 8: The distributions of the electromagnetic calibration constants at $\theta = 20^\circ$ obtained using the flat filter method for JINR, ANL, IFA and all modules (bottom-right) at full statistics.

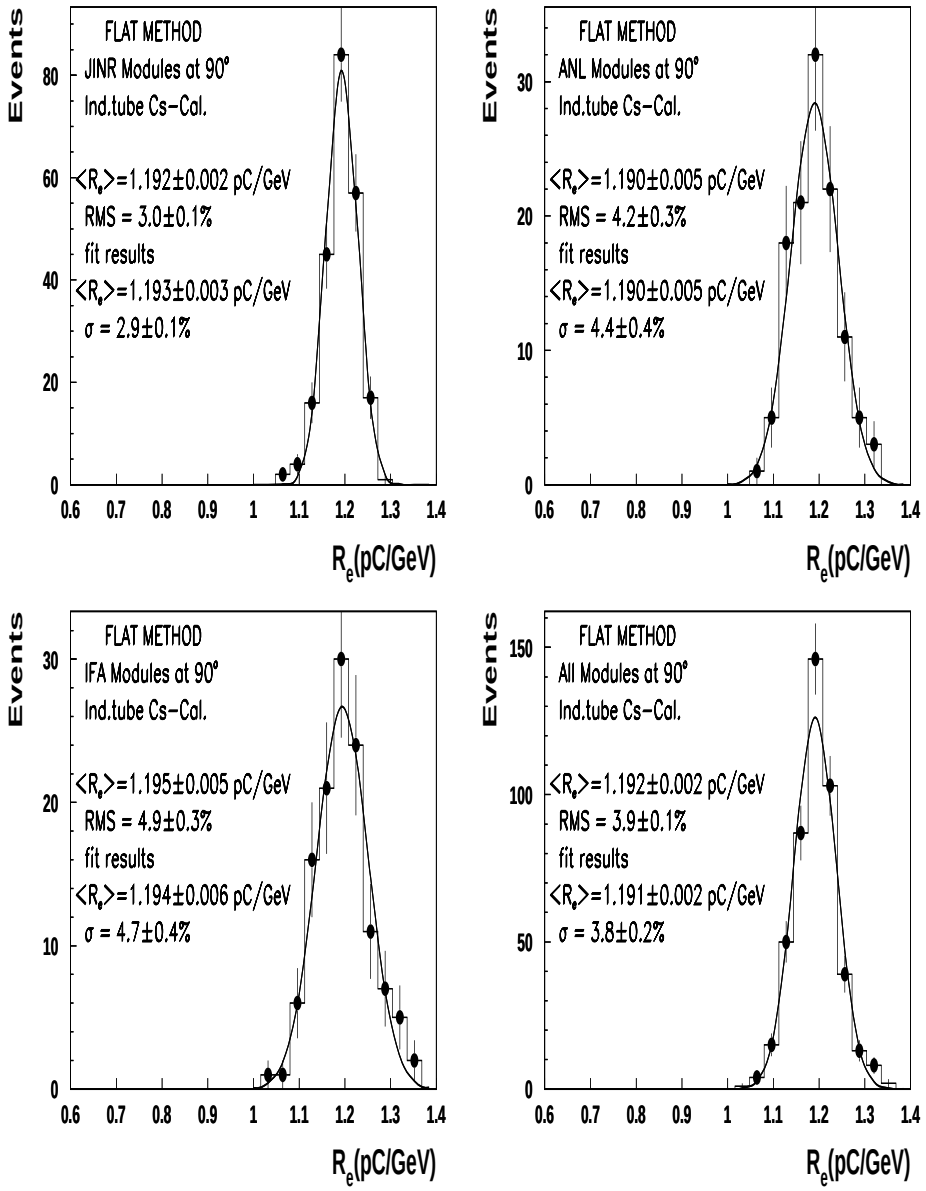

Figure 9: The distributions of the electromagnetic calibration constants at $\theta = 90°$ obtained using the flat filter method for JINR, ANL, IFA and all modules (bottom-right) at the full statistics.

The mean calibration constant and RMS for all modules amounts to 1.154 ± 0.002 pC/GeV and $2.6 \pm 0.1\%$ for the 20° electron beams. The RMS values for individual module families are shown in Table 4. The worse uniformity of ANL modules for 20° electron beam is due to the way the tiles were pre-selected for the module instrumentation[3].

6.3 Weighted averages for individual modules

The distributions of the average electromagnetic calibration constants for the fit method at 20° and 90° as a function of a module are shown in Fig. 10 (limited statistics).

Fig. 10 (top) demonstrates the mean electromagnetic calibration constants for separate modules for the fit method at 20° as a function of a module number. The weighted average value is equal to 1.033 ± 0.004 pC/GeV, the upper spread is 0.5%, the lower one is 2.6% (without the ANL-03 module).

Fig. 10 (bottom) shows the mean electromagnetic calibration constants for separate modules for the fit method at 90° as a function of a module. The weighted average value is equal to 1.068 ± 0.005 pC/GeV, the upper spread is 3.3%, the lower one is 3.4%.

The distributions of the weighted average electromagnetic calibration constants for the flat filter method at 20° and 90° as a function of a module are shown in Fig. 11.

Fig. 11 (top) demonstrates the mean electromagnetic calibration constants for separate modules for the flat filter method at 20° as a function of a module. The weighted average value is equal to 1.153 ± 0.003 pC/GeV, the upper spread is 1.6%, the lower one is 3.0% (without the ANL-03 module).

Fig. 11 (bottom) shows the mean electromagnetic calibration constants for separate modules for the flat filter method at 90° as a function of a module without (circles) and with the individual Cs tilerow correction (squares). The weighted average value is equal to 1.196 ± 0.003 pC/GeV, the upper spread is 2.2%, the lower one is 4.7%.

For determining of the weighted average values we have fitted these distributions by straight lines. If $\chi^2/(N-1)$ of the fit is greater than unit

[3]The best quality tiles were used in the barrel modules, the medium quality ones in IFA modules. The tiles used in ANL modules thus represent the lower tail of optical quality with bigger spread, which corresponds to worse RMS.

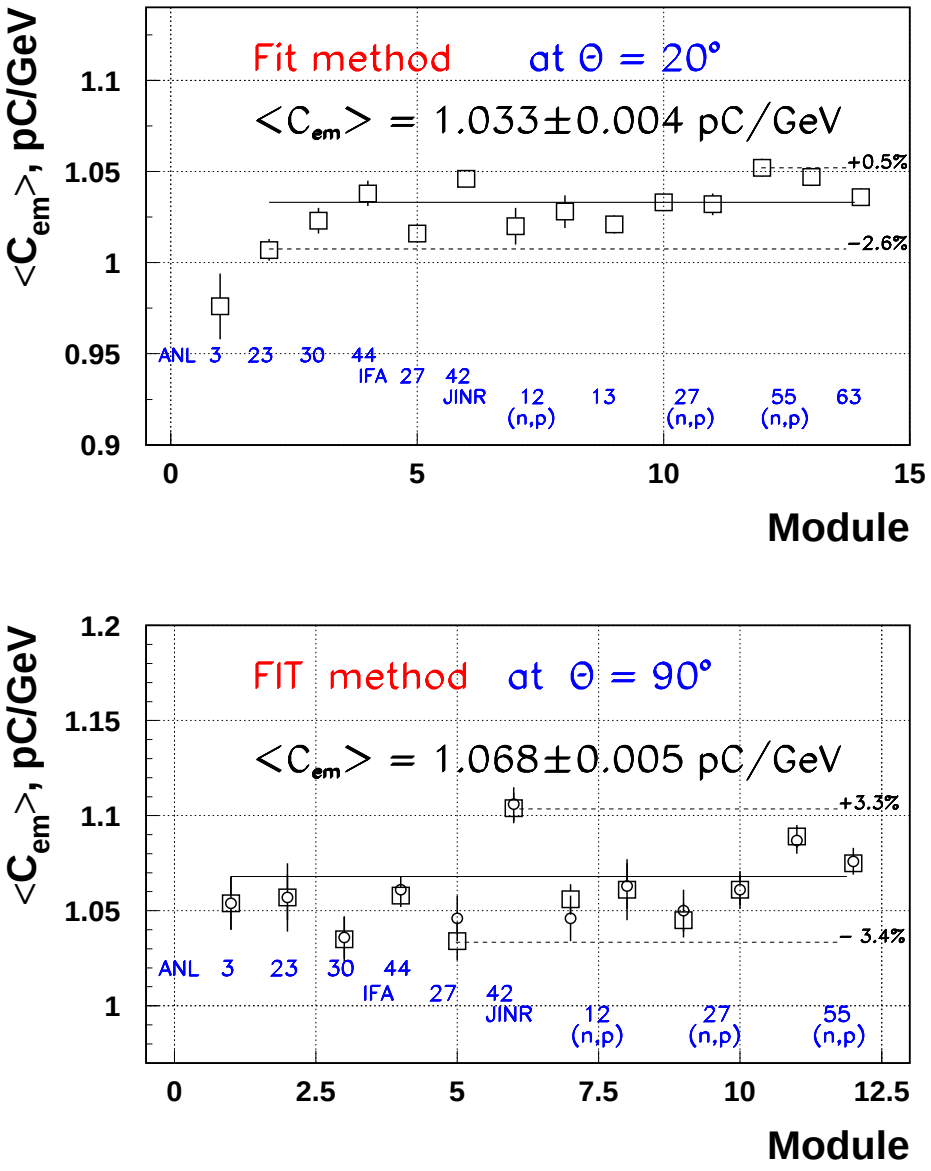

Figure 10: Top: The mean electromagnetic calibration constants for the fit method at 20° as a function of a module. Bottom: The mean electromagnetic calibration constants for the fit method at 90° as a function of a module: open circles – with the default Cs calibration, open squares – with the individual Cs tilerow correction.

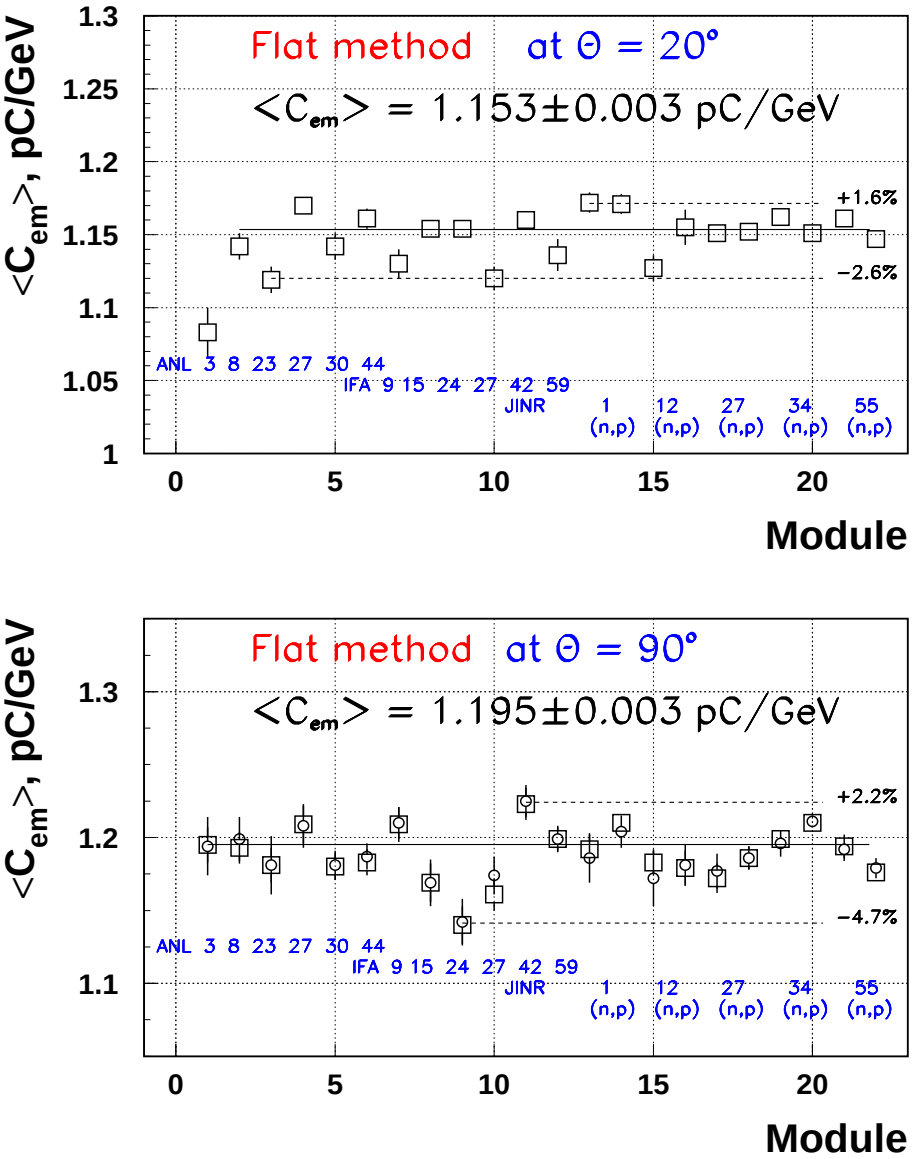

Figure 11: Top: The mean electromagnetic calibration constants for the flat filter method at 20° as a function of a module. Bottom: The mean electromagnetic calibration constants for the flat filter method at 90° as a function of a module: open circles – with the default Cs calibration, open squares – with the individual Cs tilerow correction.

(N is the number of experimental points) we increase the error obtained from the fit by a scale factor S defined as $S = \sqrt{\chi^2/(N-1)}$ according to the procedure given in Review of Particle Physics [37]. So, the weighted average values for all modules agree with the average calibration constants for separate modules within the errors.

Summary of the weighted average values of electromagnetic calibration constants extracted from Figs. 10, 11 are given in Table 5.

Table 5: The weighted average electromagnetic calibration constants (pC/GeV) and the ratios of 90°/20° and Flat/Fit methods.

Θ	Flat Method	Fit Method	Flat/Fit
20°	1.153±0.003	1.033±0.004	1.116±0.005
90°	1.195±0.003	1.068±0.005	1.119±0.006
90°/20°	1.036±0.004	1.034±0.006	

The calibration constants for 90° are larger than the corresponding ones for 20°. This is explained by the transition effect [18, 40]. The 90°/20° ratios are equal to 1.036 ± 0.004 and 1.034 ± 0.006 for the flat and fit methods.

The calibration constants for the flat method are greater than the corresponding ones for the fit method. The flat/fit ratios are equal to 1.116 ± 0.005 and 1.119 ± 0.006 for 20° and 90°. Using these values it is possible to transfer constants obtained by one method to corresponding constants obtained by other method.

7 Uniformity

The electromagnetic calibration constants, as obtained during all test-beam periods, were presented in Sections 6.1 and 6.2. The uniformity issues are addressed in this Section.

7.1 Uniformity at 20° and 90°

The RMS of the electromagnetic calibration constants at 90° with default Cs calibration is bigger than that at 20° (see Table 7 in Appendix A).

This difference reflects the cell readout structure. Since the electromagnetic showers initiated by 20° electron beams hit all tilerows in the impact cells, the tilerow-to-tilerow variations are averaged over in the sum. This is not the case of the 90° beams, where only the impact tilerow contributes to the measured signal.

The Cs calibration correction are applied to account for the tilerow-to-tilerow response variations in a cell for the 90° beams. The following formula is used:

$$R_e^{corr} = R_e \cdot \frac{A_{mean}}{A_i} \ , \tag{6}$$

where R_e (R_e^{corr}) is an electromagnetic calibration constant for given tilerow with the default cesium calibration (with the individual tilerow correction). A_{mean} is the mean amplitude of the cesium calibration for given cell, A_i is the amplitude of the cesium calibration for given tilerow in a cell, $i = 1,\ n$, where n is a number of tilerow in a cell. The values of A_i were taken from the TileCal Cs-calibration data base [35]. The changes of the average calibration constants after this correction are small. However, the RMS improves when the individual tilerow corrections are applied (see Section 7.1.1).

7.1.1 Example of an impact of the individual tilerow Cs-corrections

Let us demonstrate the impact of the individual tilerow Cs-corrections for the module JINR-34 as an example. Fig. 12 shows the distributions of the electromagnetic calibration constants for the flat filter method for this module at 20 and 180 GeV at 90°. One can see the larger spread of the constants (RMS $= 3.4 \pm 0.5\%$) in the negative part of the module in comparison with the positive part (RMS $= 1.5 \pm 0.2\%$). After applying the above-mentioned corrections the spreads became equal within the errors — $1.9 \pm 0.3\%$ and $1.6 \pm 0.2\%$, respectively (see Table 7 in Appendix A).

7.1.2 Uniformity at the module level

Let us demonstrate the module-to-module uniformity using the averages of calibrations constants obtained at 20° and 90°. Keep in mind that the results for fit method involve only limited statistics (approximately

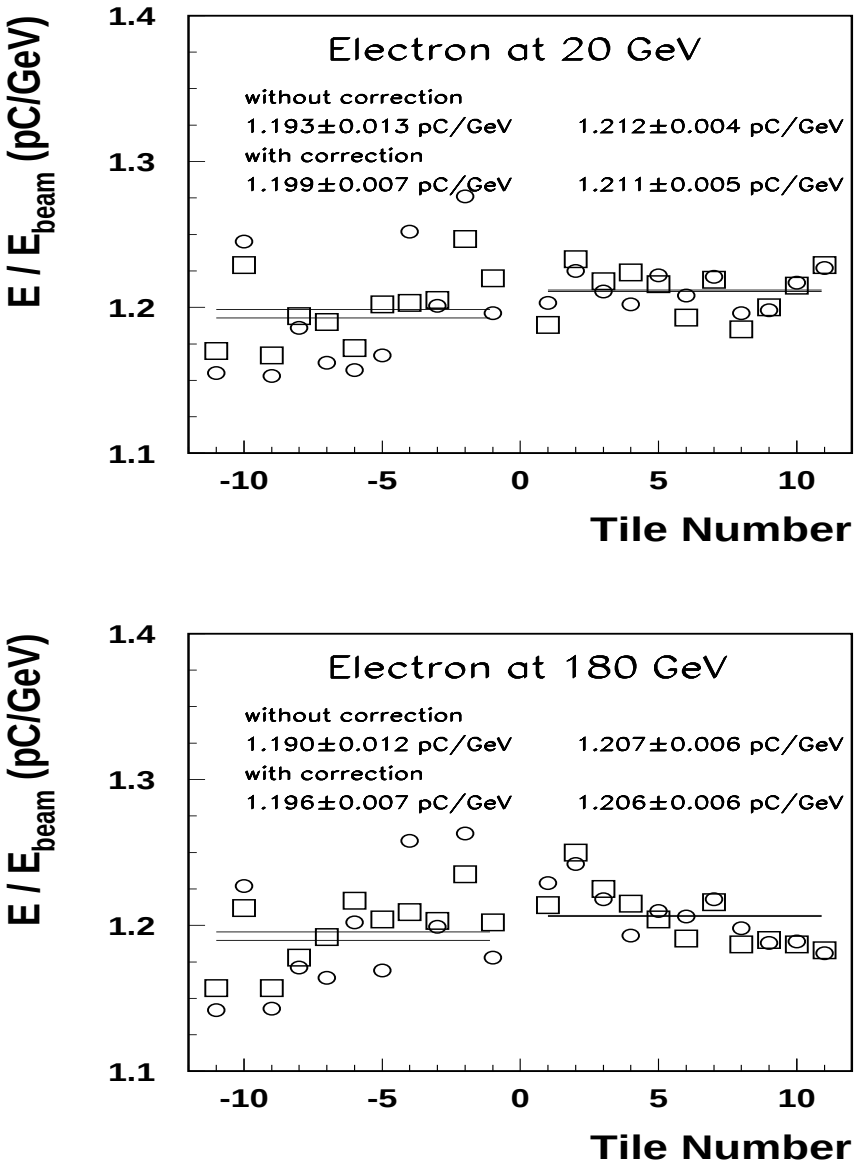

Figure 12: The electromagnetic calibration constants for JINR-34 (TB-06-2002) at 20 GeV (top) and 180 GeV (bottom) at 90° as a function of a tilerow number for the flat filter method [11]. The open circles are calibration constants with the default Cs calibration, the open squares – with the individual Cs tilerow correction.

one half of all 11% modules tested with beams) as already mentioned in Section 6.1.

The RMS values of the electromagnetic calibration constants for the flat filter method at 20° and 90° as a function of a module number are given in Table 6 and shown in the Fig. 13. The RMS values at 20° in average equal to $1.9 \pm 0.1\%$ and are systematically smaller than those at 90° (average equal to $2.7 \pm 0.2\%$).

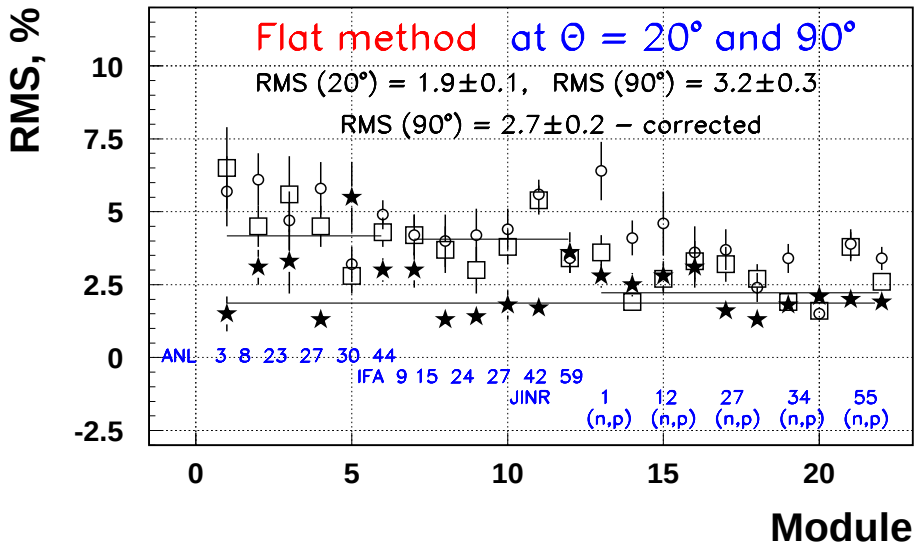

Figure 13: The RMS (%) values of the electromagnetic calibration constants for the flat filter method at 20° (black stars) and a 90° (open circles – with the default Cs calibration, open squares – with the individual Cs tilerow correction) as a function of a module number.

The RMS values for the electromagnetic calibration constants for the fit method at 20° and 90° as a function of a module number are shown on the Fig. 14. The RMS values at 20° in average equal to $2.1 \pm 0.2\%$ and are systematically smaller than those at 90° (average equal to $3.1 \pm 0.3\%$). These results at limited statistics agree with those obtained with flat filter at full statistics.

7.1.3 Uniformity at the cell level

The summary of the cell-to-cell uniformity can be deduced from the Tables 2 (fit method, limited statistics) and 4 (flat filter, full statistics).

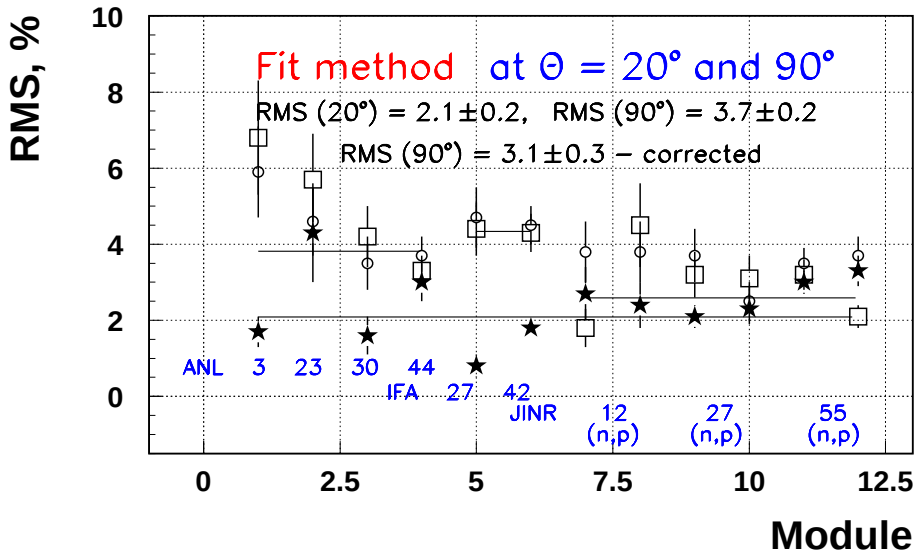

Figure 14: The RMS values (%) of the electromagnetic calibration constants for the fit method at 20° (black stars) and at 90° (open circles – with the default Cs calibration, open squares – with the individual Cs tilerow correction) as a function of a module number.

The same quantities can also be derived from Figures 7, 8, 9.

Taking into account only the results with full statistics, the uniformity amounts to $2.6 \pm 0.1\%$ at 20° and $3.9 \pm 0.1\%$ at 90° (after the individual tilerow Cs-corrections).

The results shown in Table 7 (see Appendix A) clearly indicate that the individual tilerow Cs-corrections have an appreciable effect on the resulting RMS only in the barrel modules (JINR: RMS $= 2.2 \pm 0.2\%$), but not in extended barrel ones (ANL: RMS $= 4.2 \pm 0.4\%$, IFA: RMS $= 4.1 \pm 0.4\%$). The worse correlation electron/cesium in the extended barrel modules can be explained by the fact that extended barrel modules have much deeper cells (as seen at 90°) and the electromagnetic shower reaches only part of the cell. The cell non-uniformities due to optics and instrumentation effects are only partially seen by electrons (the electron shower extends to a part of the cell), while the cesium takes into account all the tiles inside the cell.

7.1.4 Interpretation of RMS values

The results of the instrumentation of the TileCal production modules are summarized in Ref. [36]. The reported average tile-to-tile non-uniformity for barrel modules amounts to approximately $\mathrm{RMS_{unif}} = 6\%$.

According to [37], 90% of the electromagnetic shower energy is contained inside of a cylinder with the Moliere radius R_M. In our case $R_M = 20.5$ mm [38] and a period of the calorimeter containing one scintillator tile is 18 mm. The most of an electromagnetic shower passes only $N = 6$ tiles from typically 48 available in an A-cell. Thus, $\mathrm{RMS} = \frac{\mathrm{RMS_{unif}}}{\sqrt{N}} = 2.4\%$. This number should be compared with the measured non-uniformity for 20° electron beams $\mathrm{RMS} = 2.6 \pm 0.1\%$.

7.1.5 Comparison with muons results

The non-uniformity observed with electrons at 90° can be compared to that observed with muons. Fig. 15 (left) shows the mean muon response

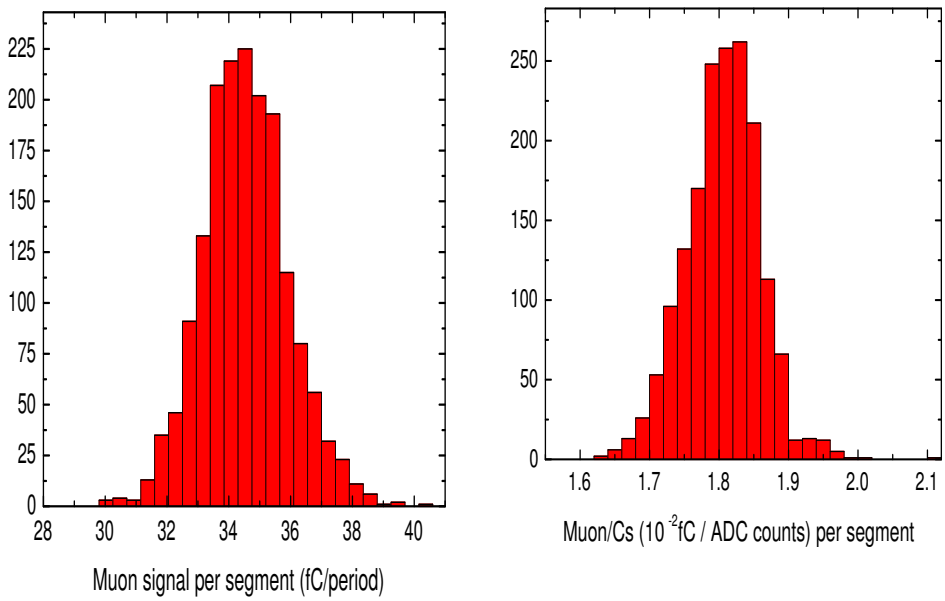

Figure 15: Left: Muon response over all tile row segments with RMS equal to 4% [39]. Right: Muon signal corrected to Cs for individual tile row responses in a given cell with RMS equal to 3% [39].

over all tilerow segments without individual tilerow correction. In this

case the RMS is equal to 4% [39]. Fig. 15 (right) shows the mean muon response over all tilerow segments with individual tilerow correction. In this case the RMS is equal to 3% [39]. As can be seen from Fig. 15 (right) and Fig. 14 the RMS spreads for muons and electrons are similar only for barrel modules. Unlike electrons, no major difference is observed between muon/Cs in barrel modules (smaller cells) and extended barrel modules (large cells), since both muon and Cs signals are integrated along whole cell.

7.2 Asymmetry of the positive and negative parts of barrel modules

We have investigated the asymmetry of the negative ($\eta < 0$) and positive ($\eta > 0$) parts of barrel modules. The results, the differences Δ_{em} between the corresponding calibration constants, are shown in Fig. 16. As one can see, these differences are equal to 0 within the errors. So, the asymmetry in calibration constants is absent.

7.3 Angular effect

The electron calibration constants obtained with the flat filter method at 90° are systematically higher than those obtained at 20° by about 3.5% (see Table 4). Therefore, the dependence of the electron response on the impact angle were studied in more detail.

The η-projective electron data were used for this purpose. As shown in Fig. 17, the electromagnetic calibration constant increases with the impact angle. The experimental data match the Monte-Carlo results and suggest that the dependence is due to the transition effect [18, 40]. In particular, it explains the difference between the calibration constants at 20° and 90°. The electron calibration constants are well described by the formula:

$$R_{exp} = (1.068 \pm 0.012) + (0.028 \pm 0.004) \cdot \log(\Theta) \ . \qquad (7)$$

One can use eventually this formula for calibration constant as function of Θ for correction of electron response at any different angles to $\Theta = 20°$ level.

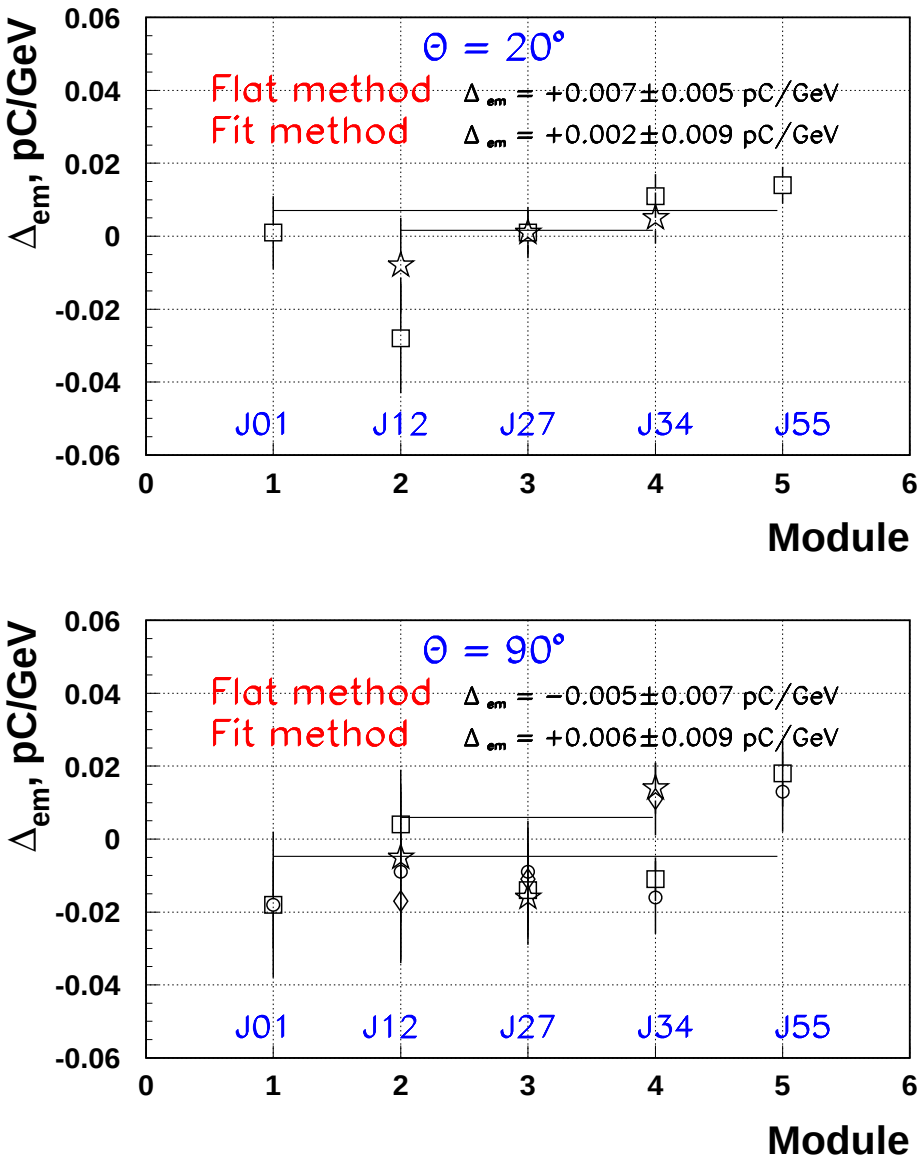

Figure 16: The asymmetry between the average calibration constants in negative and positive sides of barrel module at 20° (top) and 90° (bottom) for the flat filter method (open circles – the default Cs calibration, open squares – the individual tilerow correction) and the fit method (open diamonds – the default Cs calibration, open stars – the individual tilerow correction) as a function of a module number.

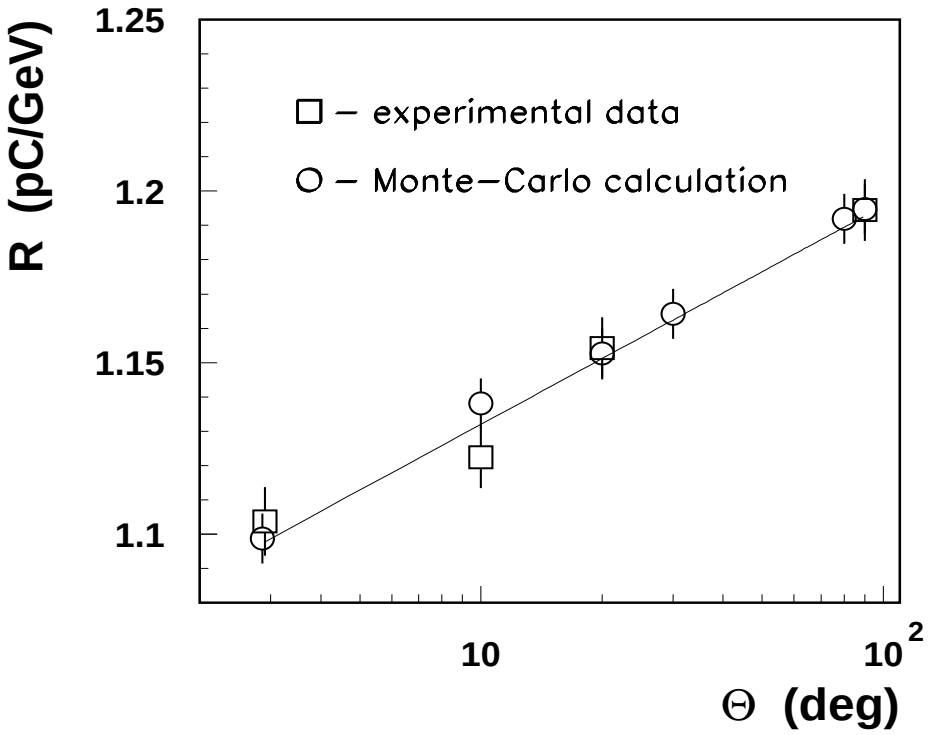

Figure 17: The electromagnetic calibration constants as a function of an impact angle. Experimental points are black squares. The GEANT4 (version 6.2) Monte-Carlo calculations for the TileCal test beam setup are indicated in open circles. The Monte-Carlo data normalized to 90° experimental result. The curve is the result of the fit experimental results by the formula (7).

7.4 Global calibration constant

The weighted average electromagnetic calibration constants from Table 5 coincide within the errors with the corresponding values obtained from the distributions of all electromagnetic calibration constants shown in Tables 4 (flat filter, full statistics) and 2 (fit method, limited statistics). Finally, we present the global constants which should be used for the electromagnetic calibration of the ATLAS Tile hadronic calorimeter data in the ATHENA framework [41]. These constants are equal to 1.15 in the case of the flat filter method and 1.04 for the fit one.

7.5 Comparison to pions response uniformity

The data from the different test beams have been used to look at the calorimeter hadronic response homogeneity after the modules have been intercalibrated with the Cs source. In this study [42] it is shown that the global uniformity of the TileCal modules is about $1.2 \pm 0.2\%$ over several η impact points (see Fig. 18). This result is in good agreement with uniformity for hadrons equal to $1.4 \pm 0.4\%$ presented in Ref. [43].

The uniformity for pions is much better than for electrons, since the hadronic shower are much extensive (broader and deeper) than the electromagnetic ones and thereby are not so sensitive to the discrete calorimeter structure as electromagnetic ones.

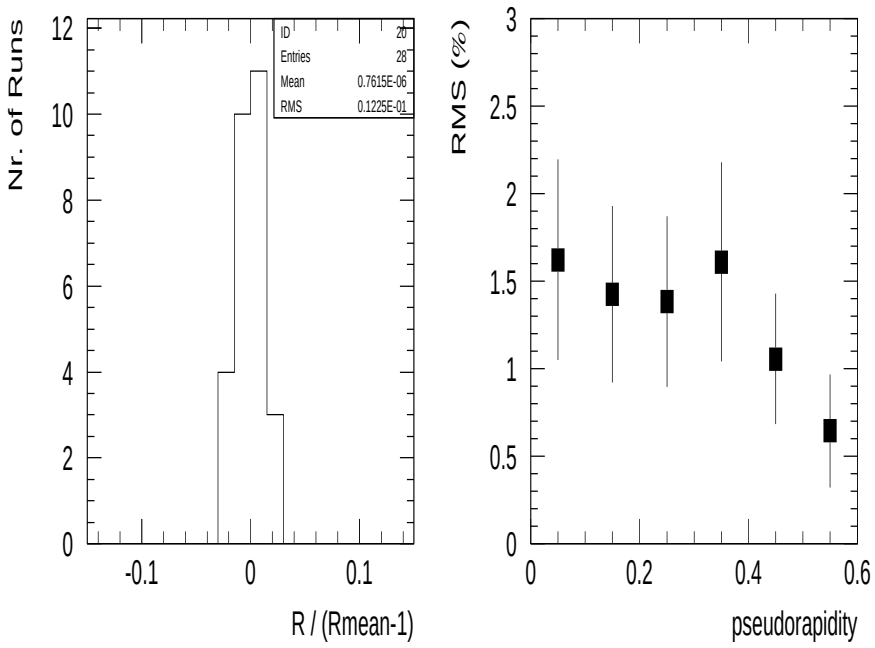

Figure 18: Calorimeter response inhomogeneity: dispersion of relative responses, $R(\eta)/(R_{mean}-1)$, for $|\eta| < 0.6$, the Test Beam data of June/July 2002 and July 2003 were used (left) and the RMS of mean response as a function of $|\eta|$ constructed using the mean response for different modules (right).

8 Conclusions

We have determined the electromagnetic calibration constants of 11% TileCal modules exposed to electron beams with incident angles of 20° and 90°. The gain of all the calorimeter cells have been pre-equalized using the radioactive Cs-source that will be also used in situ. The average values for these modules are equal to: for the flat filter method 1.154±0.002 pC/GeV and 1.192±0.002 pC/GeV for 20° and 90°, for the fit method 1.040±0.002 pC/GeV and 1.068±0.003 pC/GeV, respectively. These average values for all cells of calibrated modules agree with the weighted average calibration constants for separate modules within the errors. Using the individual calibration constants for every module the RMS spread value of constants will be 1.9±0.1%. In the case of the global constant this value will be 2.6±0.1%. Finally, we present the global constants which should be used for the electromagnetic calibration of the ATLAS Tile hadronic calorimeter data in the ATHENA framework. These constants are equal to 1.15 pC/GeV in the case of the flat filter method and 1.04 pC/GeV for the fit one.

9 Acknowledgements

This work is the result of the efforts of many people from the ATLAS TileCal Collaboration. The authors are greatly indebted to all Collaboration for test beam setup and data taking. The authors are thankful to Matteo Cavalli-Sforza, Martine Fernandez-Bosman, Ilia Korolkov, James Pilcher and Robert Stanek for a very interesting valuable discussions and important comments. We appreciate to Larry Nodulman for careful reading on this paper and useful comments.

References

[1] ATLAS Collaboration, ATLAS Technical Proposal, CERN/LHCC/94-43, 1994, CERN, Geneva, Switzerland.

[2] ATLAS Collaboration, ATLAS Detector and Physics Performance, Technical Design Report, ATLAS TDR 15, CERN/LHCC/99-15, CERN, Geneva, Switzerland.

[3] ATLAS Collaboration, ATLAS Detector and Physics Performance, Technical Design Report, ATLAS TDR 14, CERN/LHCC/99-14, p.430, CERN, Geneva, Switzerland.

[4] ATLAS Collaboration, ATLAS Calorimeter Performance, ATLAS TDR 1, CERN/LHCC/96-40, 1996, CERN, Geneva, Switzerland.

[5] ATLAS Collaboration, ATLAS Tile Calorimeter Technical Design Report, ATLAS TDR 3, CERN/LHCC/96-42, 1996, CERN, Geneva, Switzerland.

[6] R.Wigmans, Calorimetry, Energy Measurement in Particle Physics, Clarendon Press, Oxford, 2000.

[7] P.Loch, Suggestions for a General Energy Reconstruction Scheme for the ATLAS Calorimeters, ATL-CAL-97-090, CERN, Geneva, Switzerland.

[8] P.Loch, Introduction to Hadronic Calibration of the ATLAS calorimeters, Talk given on the ATLAS Calorimeter Calibration Workshop, December 2004, Tatranska Strba, Slovakia.

[9] Y.A.Kulchitsky, V.B.Vinogradov, M.V.Kuzmin, Where are Electrons? (August 2001 Test Beam), Talk given on the ATLAS TileCal analysis meeting, 14 October 2001, CERN, Geneva, Switzerland.

[10] J.A.Budagov, Y.A.Kulchitsky, V.B.Vinogradov et al., Electron and Pion Calibrations of the ATLAS TileCal Modules (September 2001), ATL-TileCal-2003-005, CERN, Geneva, Switzerland; JINR-E1-2003-22 (2003) Dubna, Russia.

[11] Y.A.Kulchitsky, Electron calibration of the TileCal Modules (June 2002). Talk given on the ATLAS TileCal analysis meeting, 17 February 2003, CERN, Geneva, Switzerland.

[12] J.A.Budagov, Y.A.Kulchitsky, V.B.Vinogradov et al, Electromagnetic Energy Calibration of the TileCal Modules with the Flat Filter Method (July 2002), ATL-TileCal-PUB-2005-003, CERN, Geneva, Switzerland.

[13] Y.A.Kulchitsky, P.V.Tsiareshka, V.B.Vinogradov, Electromagnetic Energy Calibration of the TileCal Modules with the fit Method (July 2002), ATL-TileCal-PUB-2005-005, CERN, Geneva, Switzerland.

[14] Y.A.Kulchitsky, Electron calibration of the TileCal Modules (August 2002 Test Beam). Talk given on the ATLAS TileCal analysis meeting, 23 June 2003, CERN, Geneva, Switzerland.

[15] Y.A.Kulchitsky, P.V.Tsiareshka, Energy calibration of the TileCal Modules at 180 GeV (June 2003). Talk given on the ATLAS TileCal analysis meeting, 21 June 2004, CERN, Geneva, Switzerland.

[16] Y.A.Kulchitsky, Electron calibration of the TileCal Modules at 90° (July 2003). Talk given on the ATLAS TileCal analysis meeting, 17.11.2003, CERN, Geneva, Switzerland.

[17] Y.A.Kulchitsky, V.B.Vinogradov, Electron calibration of TileCal Modules at 20° (July 2003), Talk given on the ATLAS TileCal analysis meeting, 23 February 2004, CERN, Geneva, Switzerland.

[18] Y.A.Kulchitsky, V.B.Vinogradov, Performances of the ATLAS Hadronic Tile Calorimeter Modules for Electrons and Pions, ATL-TileCal-2004-013, CERN, Geneva, Switzerland.

[19] Y.A.Kulchitsky, V.B.Vinogradov, Calibration of the Tile calorimeter in the electromagnetic energy scale, Talk given on the ATLAS Calorimeter Calibration Workshop, December 2004, Tatranska Strba, Slovakia.

[20] Y.A.Kulchitsky, Electromagnetic cell level calibration of the ATLAS Tile calorimeter modules, Talk given on the ATLAS Calorimeter Calibration Workshop, 5 – 8 September 2006, Barcelona, Spaine.

[21] L.Pribyl, J.Kvita, Electron response of 20, 50 and 180 GeV, Talk given on the ATLAS TileCal analysis meeting, 15.10.2001, CERN, Geneva, Switzerland.

[22] L.Pribyl, Response of Tilecal to Electrons at 20° and 90°. Talk given on the ATLAS TileCal analysis meeting, 7 October 2002, CERN, Geneva, Switzerland.

[23] L.Pribyl, Comparison Fit and Flat filter methods. Talk given on the ATLAS TileCal analysis meeting, 23 June 2003, CERN, Geneva, Switzerland.

[24] F.Sarri, August 2003 testbeam electron results, Talk given on the ATLAS TileCal analysis meeting, 23 February 2004, CERN, Geneva, Switzerland.

[25] A.Christov, Response of Production Modules of the ATLAS Tile Calorimeter to Electrons, ATL-TileCal-PUB-2005-009, CERN, Geneva, Switzerland.

[26] Energy reconstruction algorithms: http://tilecal.web.cern.ch/tilecal/Testbeam/documents/method_summary/

[27] R.Teuscher, T.Davidek, Methods of Energy Reconstruction in TileCal, Talk given on the TileCal analysis meeting, 06.2003, CERN, Geneva, Switzerland.

[28] S.Akhmadaliev et al., NIM A480 (2002) 508.

[29] Y.A.Kulchitsky, V.B.Vinogradov, NIM A502 (2003) 708.

[30] M.Bosman, Y.A.Kulchitsky, M.Nessi, Charged Pion Energy Reconstruction in the ATLAS Barrel Calorimeter, ATL-TileCal-2000-002, CERN, Geneva, Switzerland; JINR-E1-2000-31 (2000) JINR, Dubna, Russia.

[31] Y.A.Kulchitsky, V.B.Vinogradov, NIM A502 (2003) 775.

[32] P.Amaral et al., NIM A443 (2000) 51.

[33] P.Amaral et al., Eur.Phys.J. C20 (2001) 487.

[34] J.A.Budagov, Y.A.Kulchitsky, V.B.Vinogradov et al., Electron Response and e/h ratio of the ATLAS barrel hadron prototype calorimeter, ATL-TileCal-96-072, CERN, Geneva, Switzerland; JINR-E1-95-513 (1995) Dubna, Russia.

[35] A.Solodkov et al., Run of Cesium calibration Information Database, http://tileinfo.web.cern.ch/tileinfo/csinfo.php

[36] A.Henriques (for the ATLAS Tilecal Collaboration), Status of the ATLAS Tile hadronic calorimeter production, Prepared for 10th International Conference on Calorimetry in High Energy Physics (CALOR 2002), Pasadena, California, USA, 25-30 Mar 2002. Published in Pasadena 2002, "Calorimetry in particle physics" 532-537.

[37] Particle Data Group, Phys. Letters B592 (2004) 1.

[38] J.A.Budagov, Y.A.Kulchitsky, V.B.Vinogradov et al., Study of the hadron shower profiles with the ATLAS TILE hadron calorimeter, ATL-TILECAL-97-127, CERN, Geneva, Switzerland.

[39] O.Salto, Calibration of the hadronic calorimeter of ATLAS with transversal muons, Diploma Thetis, Barcelona, 2004.

[40] J.Budagov, A.Henriques, G.Khoriauli, J.Khubua, Y.Kulchitsky, N.Rusakovitch, P.Tsiareshka, V.Vinogradov, Study of the Transition Effect with the ATLAS TileCa, ATL-TILECAL-PUB-2006-005; ATL-COM-TILECAL-2006-007, CERN, Geneva, Switzerland.

[41] ATLAS Collaboration, ATLAS Computing TDR, ATLAS TDR-017, CERN-LHCC-2005-022, CERN, Geneva, Switzerland.

[42] J.Alexovic, G.Arabidze, M.Cavalli-Sforza, S.Constatinescu, T.Davidek, S.Dita, M.Hurwitz, L.Lovas, A.Lupi, Y.Kulchitsky, J.Pilcher, R.Stanek, I.Sykora, S.Tokar, I.Vivarelli, T.Zenis; Response Studies of Tile Calorimeter Production Modules to Pions; will be publiushed in ATLAS note. Talk given on the TileCal Performance Applications analysis meeting, 20.02.2006, CERN, Geneva, Switzerland.

[43] M.Hurwitz, Module-to-module uniformity at 180 GeV in 2002 – 2003 TileCal calibration testbeams, ATL-TILECAL-PUB-2006-008, ATL-COM-TILECAL-2006-011, CERN, Geneva, Switzerland.

Appendices

A Summary tables for test beam periods

Table 6: The summary of the average electromagnetic calibration constants in (pC/GeV) for ANL, IFA and JINR modules exposed to electron beams. (Symbols **n** and **p** denote negative ($\eta < 0$) and positive ($\eta > 0$) parts of barrel modules.)

Mod.	Flat method			Fit method		
	20°	90°		20°	90°	
		Default	Corrected		Default	Corrected
ANL-03	1.083±0.017	1.194±0.017	1.195±0.012	0.976±0.018	1.054±0.014	1.054±0.014
ANL-08	1.142±0.009	1.199±0.015	1.193±0.011			
ANL-23	1.119±0.009	1.181±0.020	1.181±0.012	1.007±0.006	1.057±0.018	1.057±0.012
ANL-27	1.170±0.005	1.208±0.015	1.209±0.013			
ANL-30	1.142±0.009	1.181±0.010	1.180±0.009	1.023±0.007	1.036±0.011	1.035±0.012
ANL-44	1.161±0.007	1.187±0.009	1.183±0.009	1.038±0.007	1.061±0.007	1.058±0.006
ANL	1.150±0.005	1.194±0.006	1.190±0.005	1.024±0.004	1.054±0.006	1.052±0.005
IFA-09	1.130±0.010	1.210±0.011	1.209±0.012			
IFA-15	1.154±0.005	1.169±0.016	1.169±0.013			
IFA-24	1.154±0.005	1.142±0.016	1.140±0.013			
IFA-27	1.120±0.008	1.174±0.013	1.161±0.011	1.016±0.005	1.046±0.012	1.034±0.010
IFA-42	1.160±0.004	1.225±0.011	1.223±0.011	1.046±0.004	1.106±0.009	1.104±0.008
IFA-59	1.136±0.011	1.199±0.008	1.199±0.009			
IFA	1.147±0.003	1.195±0.006	1.203±0.006	1.041±0.004	1.086±0.008	1.081±0.008
JINR-01n	1.172±0.007	1.186±0.017	1.192±0.010			
JINR-01p	1.171±0.007	1.204±0.011	1.210±0.006			
Δ(n-p)	0.001±0.010	-0.018±0.020	-0.018±0.012			
JINR-12n	1.127±0.009	1.172±0.019	1.183±0.009	1.020±0.010	1.046±0.012	1.056±0.008
JINR-12p	1.155±0.012	1.181±0.014	1.179±0.012	1.028±0.009	1.063±0.012	1.061±0.016
Δ(n-p)	-0.028±0.015	-0.009±0.024	0.004±0.015	-0.008±0.013	-0.017±0.017	-0.005±0.018
JINR-13*	1.196±0.005	1.232±0.009		1.021±0.005	1.054±0.008	
JINR-27n	1.151±0.004	1.177±0.012	1.172±0.010	1.033±0.004	1.050±0.011	1.045±0.009
JINR-27p	1.152±0.004	1.186±0.008	1.186±0.008	1.032±0.006	1.061±0.008	1.061±0.010
Δ(n-p)	0.001±0.006	-0.009±0.014	-0.014±0.013	0.001±0.007	-0.011±0.014	-0.016±0.013
JINR-34n	1.162±0.004	1.196±0.009	1.199±0.005			
JINR-34p	1.151±0.005	1.211±0.004	1.210±0.003			
Δ(n-p)	0.011±0.006	-0.016±0.010	-0.011±0.006			
JINR-55n	1.161±0.004	1.192±0.008	1.194±0.008	1.052±0.005	1.087±0.007	1.089±0.006
JINR-55p	1.147±0.003	1.179±0.007	1.176±0.005	1.047±0.005	1.076±0.007	1.075±0.004
Δ(n-p)	0.014±0.005	0.013±0.011	0.018±0.009	0.005±0.007	0.011±0.010	0.014±0.007
JINR-63	1.200±0.005	1.258±0.008		1.036±0.005	1.078±0.007	
JINR	1.156±0.002	1.191±0.003	1.192±0.002	1.042±0.003	1.071±0.004	1.071±0.004
ALL	1.154±0.002	1.195±0.003	1.192±0.002	1.040±0.002	1.071±0.003	1.068±0.003

Table 7: The summary of the RMS values for the electromagnetic calibration constants in (%) for the ANL, IFA and JINR modules exposed to electron beams.

Module	Flat method			Fit method		
	20°	90°		20°	90°	
		Default	Corrected		Default	Corrected
ANL-03	3.3±1.1	4.7±1.0	4.1±1.0	4.3±1.3	4.6±0.9	4.2±0.9
ANL-08	3.1±0.6	6.1±0.9	4.5±0.7			
ANL-23	1.5±0.6	5.7±1.2	3.2±0.8	1.7±0.4	5.9±1.2	3.3±0.8
ANL-27	1.3±0.3	5.8±0.9	4.5±0.7			
ANL-30	1.7±0.6	3.2±0.6	2.8±0.6	1.6±0.5	3.5±0.7	4.2±0.8
ANL-44	3.0±0.4	4.9±0.5	4.3±0.5	3.0±0.5	3.7±0.5	3.3±0.4
ANL	3.4±0.3	5.3±0.4	4.2±0.3	3.7±0.4	3.8±0.4	3.7±0.4
IFA-09	3.0±0.6	4.2±0.7	4.2±0.7			
IFA-15	1.3±0.3	4.0±0.9	3.7±0.8			
IFA-24	1.4±0.3	4.2±0.9	3.0±0.8			
IFA-27	1.8±0.5	4.4±0.7	3.8±0.6	0.8±0.4	4.7±0.8	4.4±0.7
IFA-42	1.7±0.2	5.6±0.5	5.4±0.5	1.8±0.2	4.5±0.5	4.3±0.5
IFA-59	3.6±0.7	3.4±0.5	3.4±0.5			
IFA	2.6±0.2	4.9±0.3	4.9±0.3	2.0±0.2	5.3±0.5	5.3±0.5
JINR-01n	2.8±0.4	6.4±1.0	3.6±0.6			
JINR-01p	2.5±0.4	4.1±0.6	1.9±0.3			
JINR-12n	2.8±0.5	4.6±1.1	2.7±0.5	2.7±0.7	3.8±0.8	1.8±0.5
JINR-12p	3.1±0.7	3.6±0.9	3.3±0.7	2.4±0.6	3.8±0.8	4.5±1.1
JINR-27n	1.6±0.3	3.7±0.7	3.2±0.6	2.1±0.3	3.7±0.7	3.2±0.6
JINR-27p	1.3±0.2	2.4±0.5	2.7±0.5	2.3±0.4	2.5±0.5	3.1±0.6
JINR-34n	1.8±0.2	3.4±0.5	1.9±0.3			
JINR-34p	2.1±0.3	1.5±0.2	1.6±0.2			
JINR-55n	2.0±0.2	3.9±0.5	3.8±0.5	3.0±0.3	3.5±0.4	3.2±0.4
JINR-55p	1.9±0.2	3.4±0.4	2.6±0.3	3.3±0.4	3.7±0.5	2.1±0.3
JINR	2.3±0.1	3.9±0.2	3.0±0.1	3.1±0.2	3.7±0.3	3.3±0.2
ALL	2.6±0.1	4.5±0.2	3.9±0.1	3.0±0.1	4.3±0.2	4.0±0.2

B Figures for individual test beam periods

B.1 Test beam: 09-2001

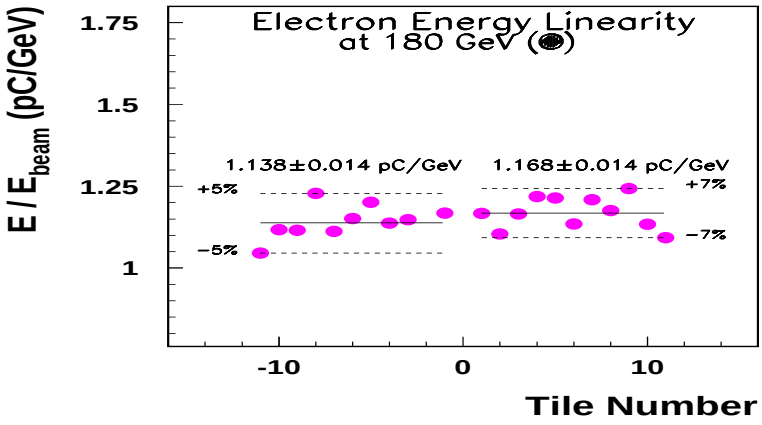

Figure 19: The electromagnetic calibration constants for TB-09-2001 for the extended barrel modules IFA-15 ($EBM+$) and IFA-24 ($EBM+$) at 180 GeV for 90° for the flat filter method as a function of a tilerow number [9].

B.2 Test beam: 06-2002

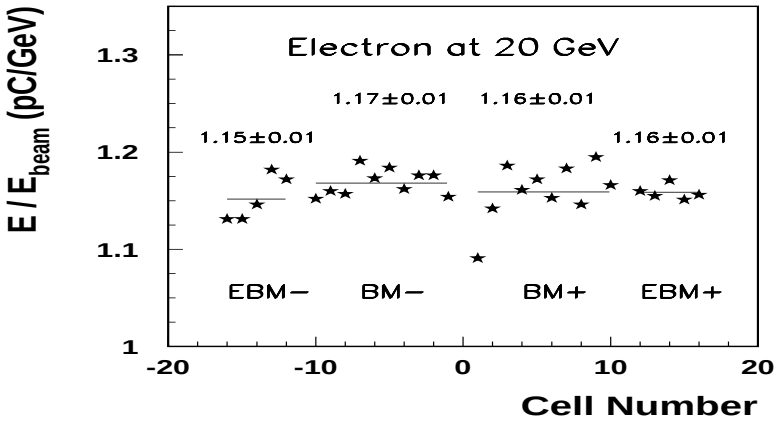

Figure 20: The electromagnetic calibration constants for TB-06-2002 at 20 GeV for 20° as a function of a A-cell number for IFA-59 ($EBM+$), ANL-08 ($EBM-$) and JINR-34 ($BM\pm$) for the flat filter method [11].

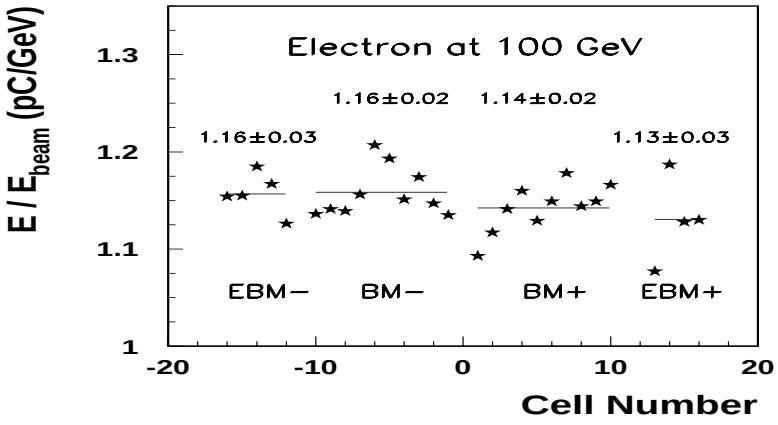

Figure 21: The electromagnetic calibration constants for TB-06-2002 at 100 GeV for 20° as a function of a A-cell number for IFA-59 ($EBM+$), ANL-08 ($EBM-$) and JINR-34 ($BM\pm$) for the flat filter method [11].

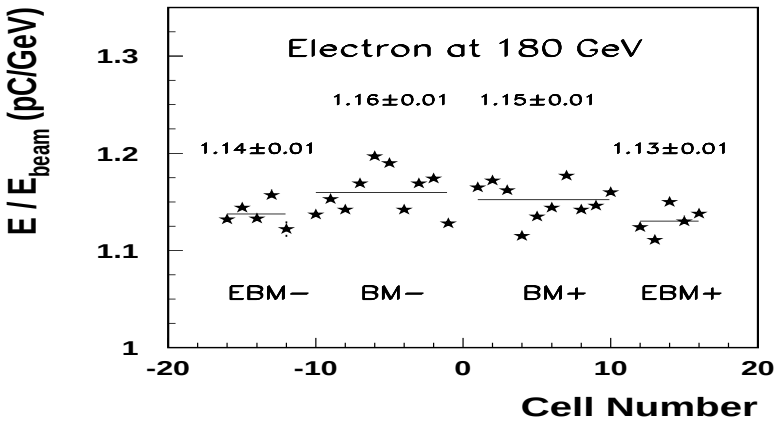

Figure 22: The electromagnetic calibration constants for TB-06-2002 at 180 GeV for 20° as a function of a A-cell number for IFA-59 ($EBM+$), ANL-08 ($EBM-$) and JINR-34 ($BM\pm$) for the flat filter method [11].

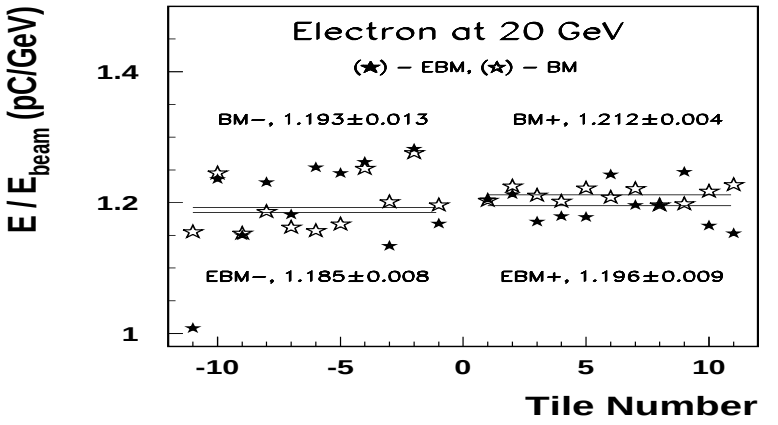

Figure 23: The electromagnetic calibration constants for TB-06-2002 at 20 GeV for 90° as a function of a tile number for IFA-59 ($EBM+$), ANL-08 ($EBM-$) and JINR-34 ($BM\pm$) for the flat filter method [11].

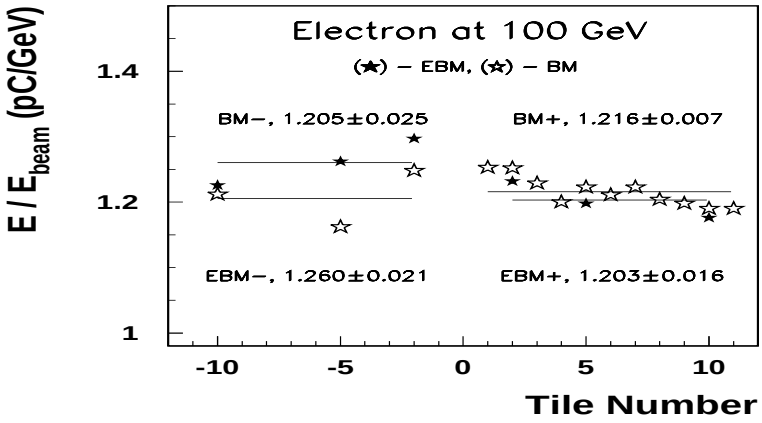

Figure 24: The electromagnetic calibration constants for TB-06-2002 at 100 GeV for 90° as a function of a tile number for IFA-59 ($EBM+$), ANL-08 ($EBM-$) and JINR-34 ($BM\pm$) for the flat filter method [11].

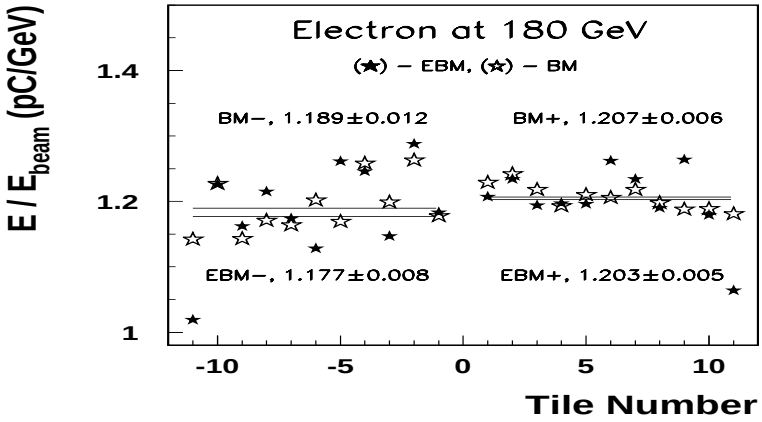

Figure 25: The electromagnetic calibration constants for TB-06-2002 at 180 GeV for 90° as a function of a tile number for IFA-59 ($EBM+$), ANL-08 ($EBM-$) and JINR-34 ($BM\pm$) for the flat filter method [11].

B.3 Test beam: 07-2002

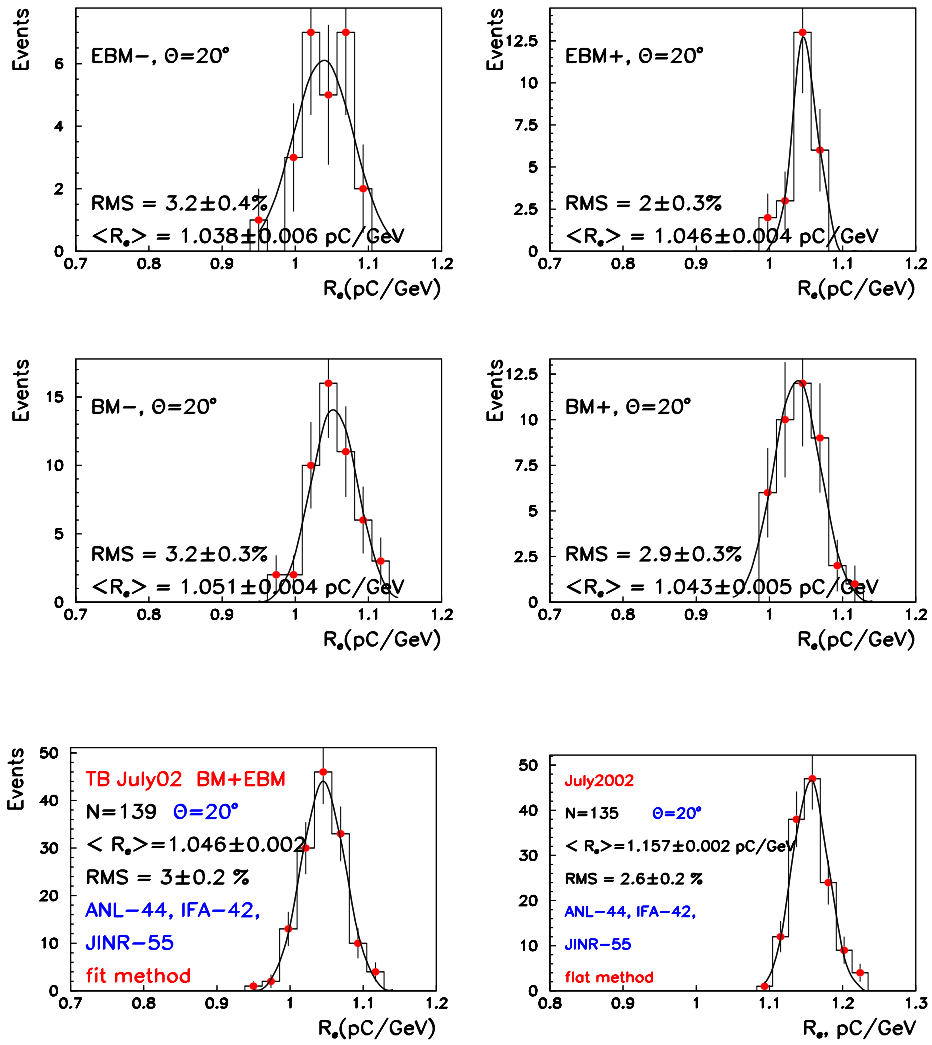

Figure 26: The distributions of the calibration constants for TB-07-2002 at $\theta = 20^\circ$ for the fit method for all energies of ANL-44 (EBM−, up-left), IFA-42 (EBM+, up-right), JINR-55− (BM−, middle-left) and JINR-55+ (BM+, middle-right), for all energies for these modules for the fit method (down-left) and the flat filter method (down-right) [13].

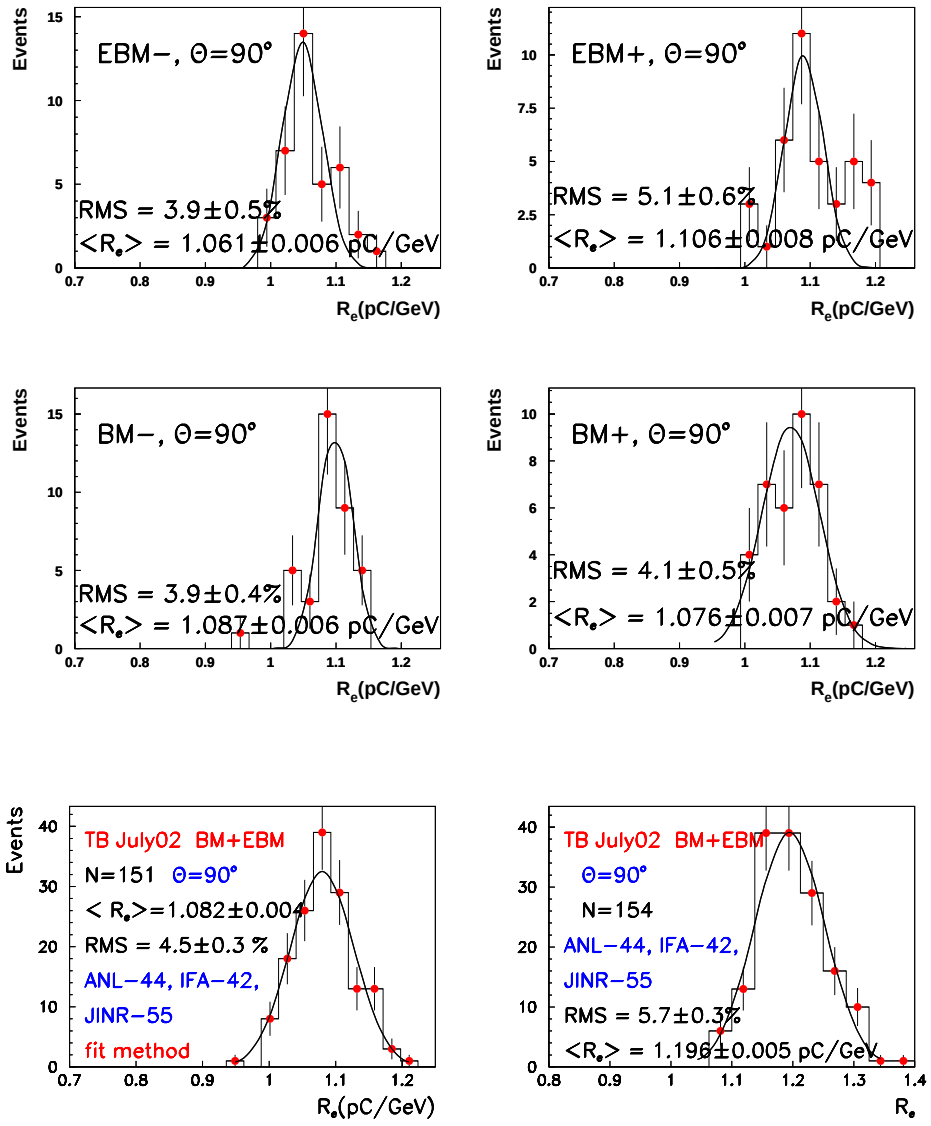

Figure 27: The distributions of the calibration constants for TB-07-2002 at $\theta = 90^\circ$ for the fit method for all energies of ANL-44 (up-left), IFA-42 (up-right), JINR-55− (middle-left) and JINR-55+ (middle-right), for all energies for these modules for the fit method (down-left) and the flat filter method (down-right) [13].

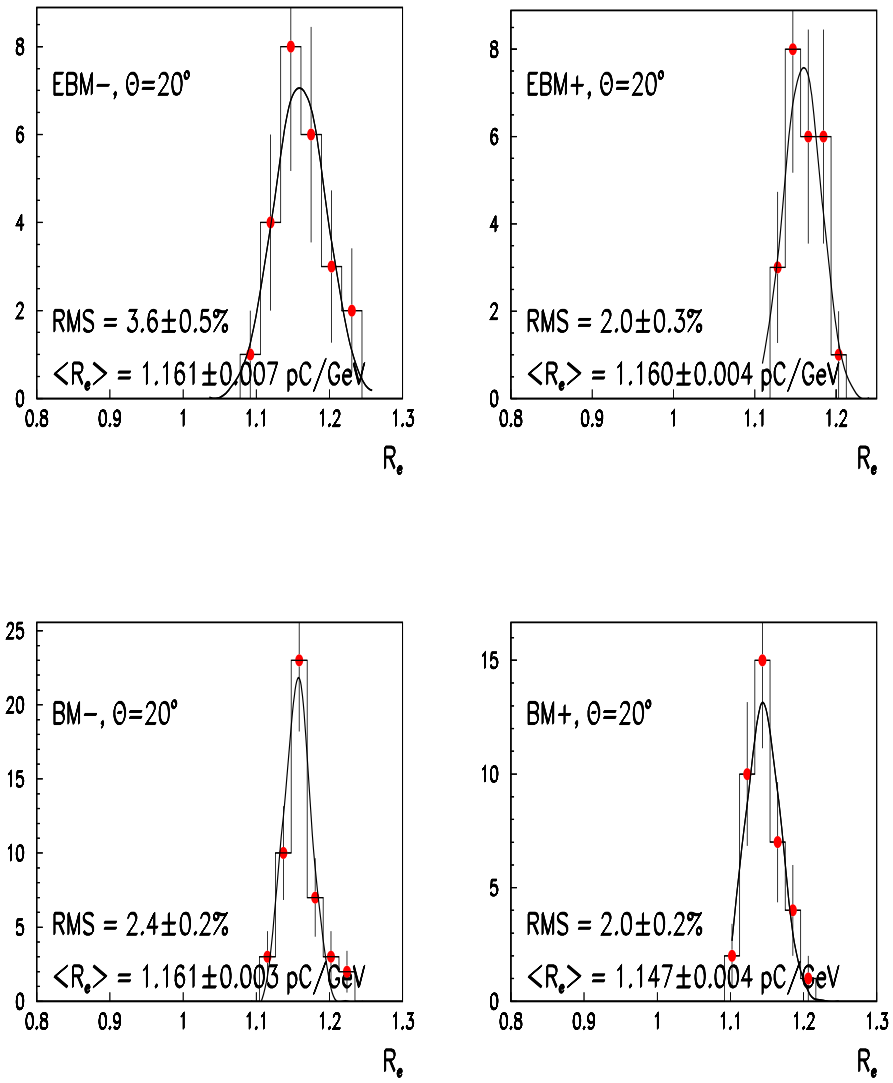

Figure 28: The distributions of the electromagnetic calibration constants (TB-07-2002) for the flat filter method at $\theta = 20°$ for all energies of ANL-44 (up-left), IFA-42 (up-right), JINR-55− (down-left) and JINR-55+ (down-right) modules [12].

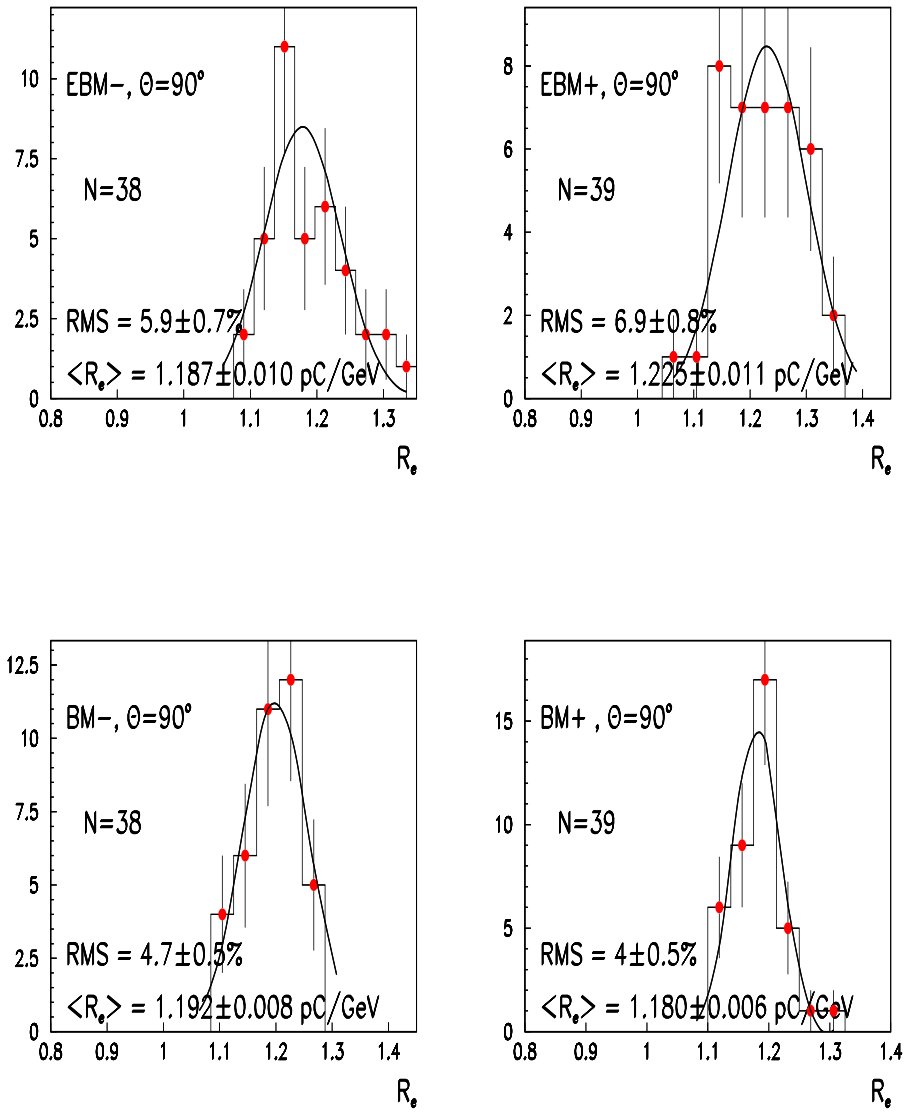

Figure 29: The distributions of the electron calibration constants (TB-07-2002) for the flat filter method at $\theta = 90°$ of ANL-44 (up-left), IFA-42 (up-right), JINR-55− (down-left) and JINR-55+ (down-right) [12].

B.4 Test beam: 08-2002

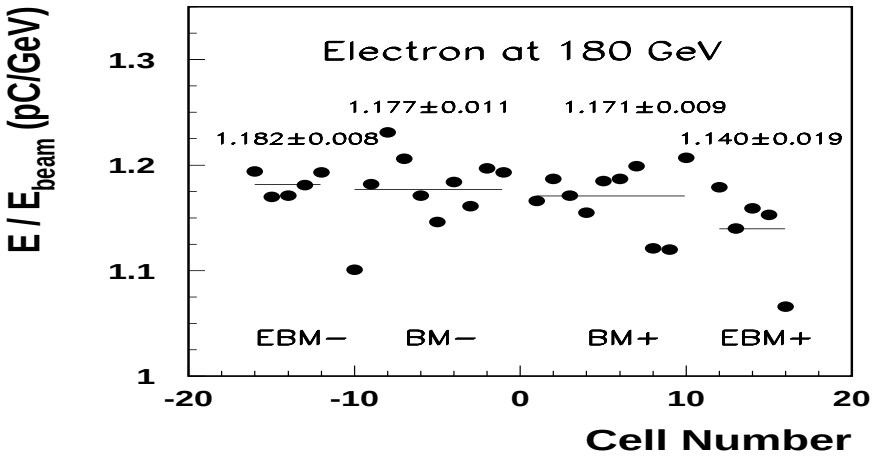

Figure 30: The electromagnetic calibration constants for TB-08-2002 at 180 GeV for 20° as a function of a A-cell number for IFA-09 ($EBM+$), ANL-27 ($EBM-$) and JINR-01 ($BM\pm$) for the flat filter method [14].

B.5 Test beam: 06-2003

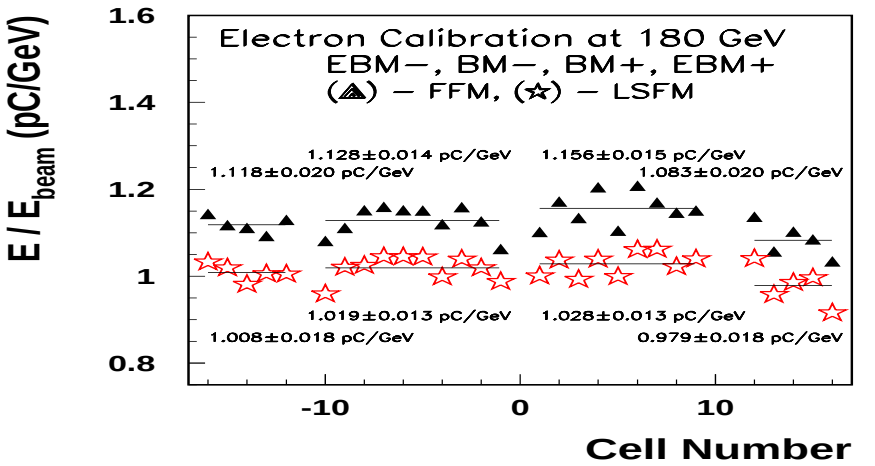

Figure 31: The electromagnetic calibration constants for TB-06-2003 at 180 GeV for 20° as a function of a A-cell number for ANL-03 ($EBM+$), ANL-23 ($EBM-$) and JINR-12 ($BM\pm$). FFM — the flat filter method. LSFM — the fit method [15].

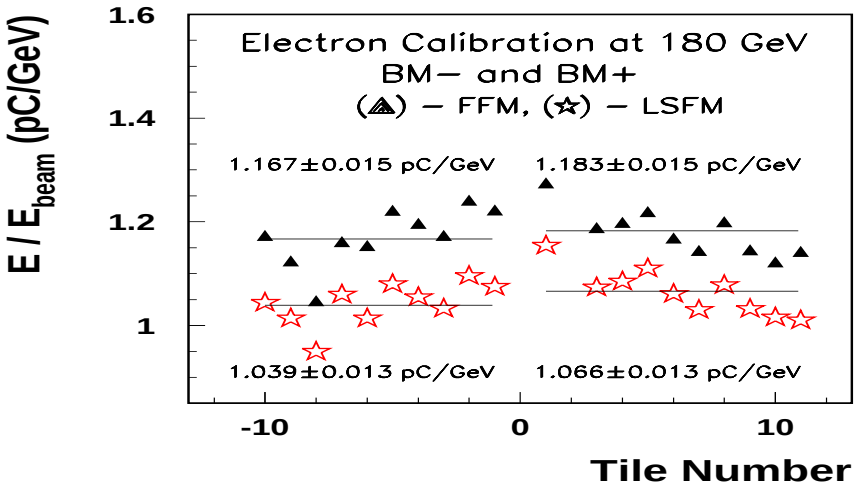

Figure 32: The electromagnetic calibration constants for TB-06-2003 at 180 GeV for 90° as a function of a tilerow number for JINR-12 ($BM\pm$) [15].

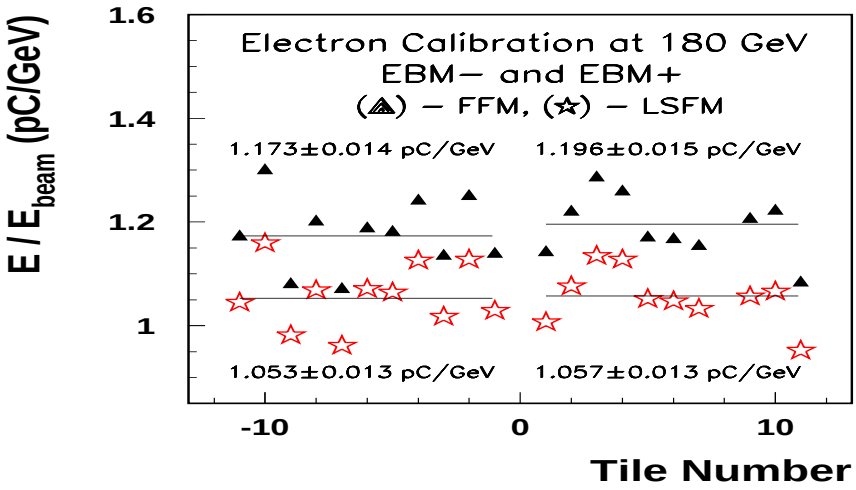

Figure 33: The electromagnetic calibration constants for TB-06-2003 at 180 GeV for 90° as a function of a tilerow number for ANL-03 ($EBM+$) and ANL-23 ($EBM-$). FFM — the flat filter method. LSFM — the fit method [15].

B.6 Test beam: 07-1-2003

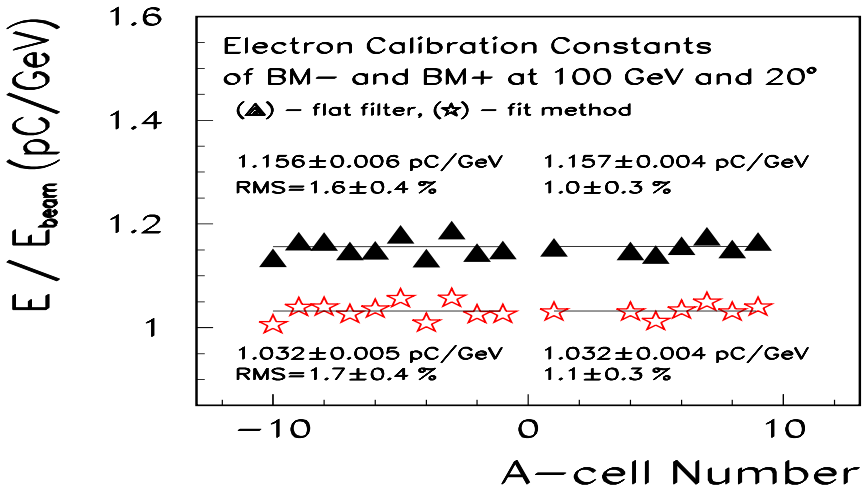

Figure 34: The electromagnetic calibration constants for JINR-27 Module for 100 GeV at 20° as a function of a A-cell number (TB-07-1-2003) [17].

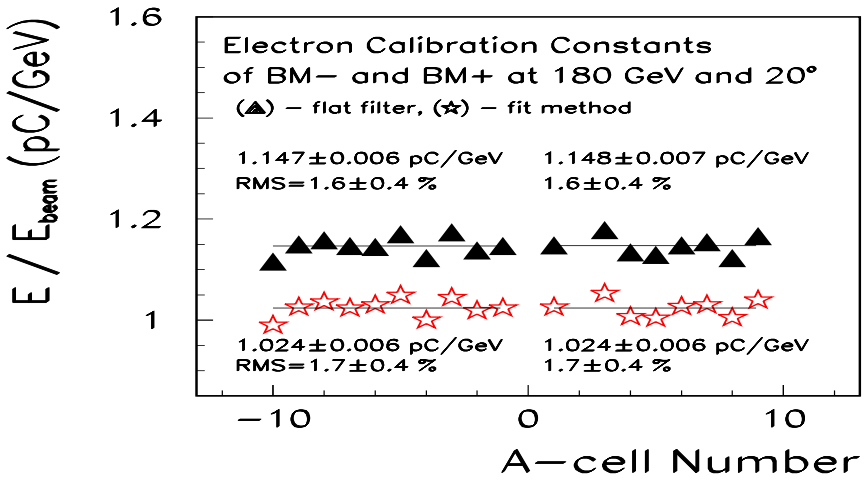

Figure 35: The electromagnetic calibration constants for JINR-27 Module for 180 GeV at 20° as a function of a A-cell number (TB-07-1-2003) [17].

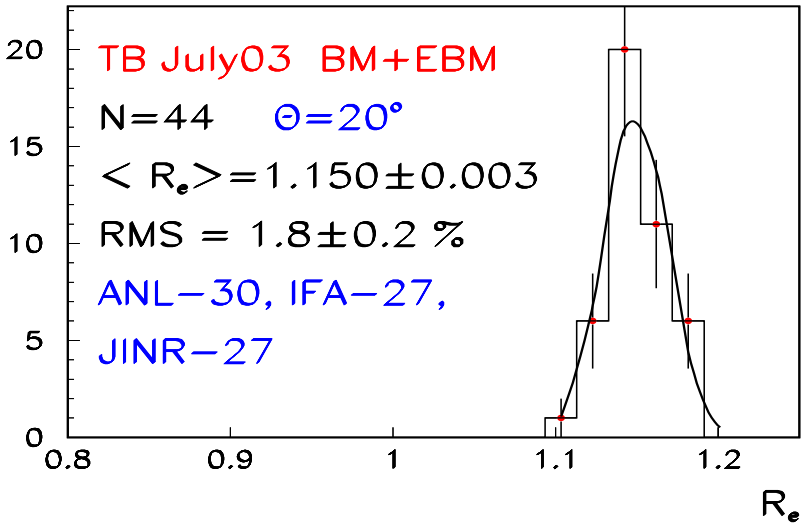

Figure 36: The distribution of the electromagnetic calibration constants for the TB-07-1-2003 at $\theta = 20^\circ$ for all energies for the modules of ANL-30, IFA-27 and JINR-27 for the flat filter method [17].

C Tables for individual test beam periods

C.1 Test beam: 09-2001

Table 8: The calibration constants (pC/GeV) for the flat filter method at $\theta = 20^\circ$ for the EBM: IFA-15 (A+12 $\div$ A+16) and IFA-24 (A$-$12 $\div$ A$-$16) (TB-09-2001) [10].

Cell	50 GeV	180 GeV	
	$+20^\circ$	-20°	$+20^\circ$
A+12	1.161±0.001	1.161±0.006	
A+13	1.145±0.002		1.155±0.001
A+14		1.125±0.002	1.155±0.001
A+15		1.179±0.002	
A+16		1.148±0.001	
mean	1.153±0.02	1.153±0.012	1.148±0.02
mean2		1.151±0.01	
A$-$12	1.166±0.003		1.175±0.005
A$-$13	1.161±0.004		1.176±0.005
A$-$14	1.147±0.004	1.139±0.001	1.164±0.004
A$-$15	1.137±0.004	1.130±0.001	1.142±0.004
A$-$16		1.137±0.001	1.172±0.004
mean	1.155±0.006	1.135±0.002	1.164±0.003
mean2		1.151±0.006	

Table 9: The 180 GeV electron calibration constants in pC/GeV for various tiles at $\theta = 90°$.

Tile	EBM− (IFA-24)(*)	EBM+ (IFA-015)
1	1.168±0.002	1.167±0.002
2		1.104±0.002
3	1.148±0.002	1.165±0.002
4	1.137±0.002	1.219±0.002
5	1.201±0.002	1.214±0.002
6	1.151±0.002	1.135±0.002
7	1.112±0.002	1.209±0.002
8	1.228±0.002	1.176±0.002
9	1.116±0.002	1.243±0.002
10	1.117±0.002	1.134±0.002
11	1.046±0.002	1.093±0.002
mean	1.14±0.01	1.17±0.01

(*) The electromagnetic calibration constants for tilerows 8 – 11 (cell D6) are systematically smaller than average for module IFA-24.

C.2 Test beam: 06-2002

Table 10: The calibration constants (pC/GeV) for the TileCal Extended Barrel Modules "ANL-08" ($\eta < 0$) and "IFA-59" ($\eta > 0$) at $\theta = 20°$ obtained using the flat filter method (TB-06-2002) [11]. Accuracy of constants is 0.005.

	20 GeV	100 GeV	180 GeV	20 GeV	100 GeV	180 GeV
Cell	EBM− (ANL-08)			EBM+ (IFA-59)		
12	1.172	1.126	1.122	1.160	—	1.124
13	1.182	1.167	1.157	1.155	1.007	1.111
14	1.146	1.185	1.033	1.171	1.187	1.150
15	1.131	1.155	1.144	1.151	1.128	1.130
16	1.131	1.154	1.132	1.156	1.130	1.138
mean	1.15 ±0.01	1.16 ±0.03	1.14 ±0.01	1.16 ±0.01	1.13 ±0.03	1.13 ±0.01

Table 11: The calibration constants (pC/GeV) for the TileCal Barrel Module "JINR-34" at $\theta = 20°$ obtained using the flat filter method (TB-06-2002) [11]. Accuracy of constants is 0.005.

	20 GeV	100 GeV	180 GeV	20 GeV	100 GeV	180 GeV
Cell	BM− (JINR-34)			BM+ (JINR-34)		
1	1.154	1.135	1.128	1.091	1.093	1.165
2	1.176	1.147	1.174	1.142	1.117	1.172
3	1.176	1.174	1.169	1.186	1.141	1.162
4	1.162	1.151	1.142	1.161	1.160	1.115
5	1.184	1.193	1.190	1.172	1.129	1.135
6	1.173	1.207	1.197	1.153	1.149	1.144
7	1.191	1.156	1.169	1.183	1.178	1.177
8	1.157	1.139	1.142	1.146	1.144	1.142
9	1.160	1.141	1.153	1.195	1.149	1.146
10	1.152	1.136	1.137	1.166	1.166	1.160
mean	1.17 ±0.01	1.16 ±0.01	1.16 ±0.01	1.16 ±0.01	1.14 ±0.01	1.15 ±0.01

Table 12: Mean Calibration Constants (pC/GeV) for TileCal Modules at 20° (TB-06-2002).

		Calibration Constants (pC/GeV)		
TileCal Module		High Gain (20 GeV)	Low Gain (100 GeV)	Low Gain (180 GeV)
ANL-08:	EBM−	1.15 ± 0.01	1.16 ± 0.03	1.14 ± 0.01
IFA-59:	EBM+	1.16 ± 0.01	1.13 ± 0.03	1.13 ± 0.01
JINR-34:	BM−	1.17 ± 0.01	1.16 ± 0.02	1.16 ± 0.01
	BM+	1.16 ± 0.01	1.14 ± 0.02	1.15 ± 0.01

Table 13: The calibration constants (pC/GeV) for the EBM "ANL-08" and "IFA-59" at $\theta = 90°$ obtained using the flat filter method (TB-06-2002) [11]. Accuracy of constants is 0.005.

	20 GeV	100 GeV	180 GeV	20 GeV	100 GeV	180 GeV
Tile	EBM− (ANL-08)			EBM+ (IFA-59)		
1	1.168	—	1.183	1.205	—	1.207
2	1.282	1.297	1.288	1.213	1.232	1.234
3	1.134	—	1.147	1.171	—	1.194
4	1.262	—	1.246	1.179	—	1.197
5	1.245	1.262	1.261	1.178	1.198	1.196
6	1.254	—	1.128	1.243	—	1.262
7	1.182	—	1.174	1.196	—	1.234
8	1.231	—	1.215	1.196	—	1.190
9	1.150	—	1.162	1.247	—	1.264
10	1.236	1.226	1.226	1.165	1.176	1.179
11	1.008	—	1.019	1.153	—	1.064
mean	1.185 ±0.026	1.260 ±0.021	1.177 ±0.024	1.196 ±0.009	1.203 ±0.016	1.203 ±0.017

Table 14: The calibration constants (pC/GeV) for the Barrel Module "JINR-34" at $\theta = 90°$ obtained using the flat filter method (TB-06-2002) [11]. Accuracy of constants is 0.005.

	20 GeV	100 GeV	180 GeV	20 GeV	100 GeV	180 GeV
Tile	BM− (JINR-34)			BM+ (JINR-34)		
1	1.196	—	1.178	1.203	1.253	1.229
2	1.276	1.248	1.263	1.225	1.252	1.242
3	1.201	—	1.199	1.211	1.229	1.218
4	1.252	—	1.258	1.202	1.200	1.193
5	1.167	1.162	1.169	1.222	1.223	1.210
6	1.157	—	1.202	1.208	1.211	1.206
7	1.162	—	1.164	1.221	1.223	1.218
8	1.186	—	1.171	1.196	1.204	1.198
9	1.153	—	1.143	1.198	1.198	1.188
10	1.245	1.212	1.227	1.217	1.190	1.189
11	1.155	—	1.142	1.227	1.190	1.181
mean	1.193 ±0.013	1.205 ±0.025	1.190 ±0.012	1.212 ±0.004	1.216 ±0.008	1.207 ±0.006

Table 15: Mean Calibration Constants (pC/GeV) for TileCal Modules ANL-08, IFA-59 and JINR-34 at 90° (TB-06-2002).

	Calibration Constants (pC/GeV)		
TileCal Module	High Gain (20 GeV)	Low Gain (100 GeV)	Low Gain (180 GeV)
ANL-08: EBM−	1.185 ± 0.026	1.260 ± 0.021	1.177 ± 0.024
IFA-59: EBM+	1.196 ± 0.009	1.203 ± 0.016	1.203 ± 0.017
JINR-34: BM−	1.193 ± 0.013	1.205 ± 0.025	1.190 ± 0.012
BM+	1.212 ± 0.004	1.216 ± 0.008	1.207 ± 0.006

C.3 Test beam: 07-2002

C.3.1 The Fit Method results

Table 16: The calibration constants (pC/GeV) for the extended barrel module EBM− (ANL-44) at $\theta = 20^\circ$ (TB-07-2002),the fit method. Accuracy of constants is 0.005.

Cell	10 GeV	20 GeV	50 GeV	100 GeV	180 GeV
A−12	1.068	1.062	1.069	1.036	1.035
A−13	1.076	1.048	1.039	1.019	1.036
A−14	1.019	1.017	0.958	0.992	1.008
A−15	1.022	1.025	1.010	1.007	1.022
A−16	1.086	1.088	1.063	1.063	1.075
mean	1.054 ±0.014	1.048 ±0.013	1.028 ±0.018	1.023 ±0.012	1.035 ±0.011
RMS, %	3.1±1	2.9±0.9	4.1±1.3	2.7±0.9	2.5±0.8

Table 17: The calibration constants (pC/GeV) for the extended barrel module EBM+ (IFA-42) at $\theta = 20^\circ$ (TB-07-2002), the fit method. Accuracy of constants is 0.005.

Cell	10 GeV	20 GeV	50 GeV	100 GeV	180 GeV
A+12	1.078	1.075	1.060	1.048	
A+13	1.057	1.054	1.060	1.040	1.052
A+14	1.061	1.060	1.051	1.029	1.041
A+15	1.047	1.045	1.023	0.993	1.004
A+16	1.048	1.055	1.045	1.025	1.043
mean	1.058 ±0.006	1.058 ±0.005	1.048 ±0.007	1.027 ±0.009	1.035 ±0.11
RMS, %	1.3±0.4	1.1±0.3	1.5±0.5	2.1±0.7	2.1±0.8

Table 18: The calibration constants (pC/GeV) for the BM− (JINR-55) barrel module at $\theta = 20^\circ$ (TB-07-2002), the fit method. Accuracy of constants is 0.005.

Cell	10 GeV	20 GeV	50 GeV	100 GeV	180 GeV
A−1	1.075	1.060	1.036	1.032	1.027
A−2	1.050	1.040	1.024	1.009	1.016
A−3	1.078	1.070	1.060	1.053	1.057
A−4	1.091	1.076	1.048	1.055	1.042
A−5	1.105	1.096	1.070	1.054	1.075
A−6	1.105	1.105	1.097	1.104	1.074
A−7	1.081	1.069	1.045	1.030	1.032
A−8	1.083	1.074	1.050	1.018	1.039
A−9	1.051	1.043	1.021	1.012	1.033
A−10	1.052	1.035	1.000	0.971	0.966
mean	1.077 ±0.006	1.067 ±0.007	1.045 ±0.009	1.034 ±0.011	1.0360 ±0.010
RMS, %	2.1±0.6	2.3±0.5	2.7±0.6	3.6±0.8	3.1±0.7

Table 19: The calibration constants (pC/GeV) for the BM+(JINR-55) barrel module at $\theta = 20^\circ$ (TB-07-2002), the fit method. Accuracy of constants is 0.005.

Cell	10 GeV	20 GeV	50 GeV	100 GeV	180 GeV
A+1	1.064	1.048	1.045	1.017	1.006
A+2	1.065	1.077		1.026	1.026
A+3					
A+4	1.062	1.022		0.989	0.987
A+5	1.076	1.056	1.039	1.030	1.036
A+6	1.073	1.058	1.047	1.037	1.033
A+7	1.082	1.063	1.047	1.024	1.027
A+8	1.054	1.031	1.025	1.001	1.006
A+9	1.100	1.122			1.177
A+10	1.080	1.056	1.048	1.005	1.048
mean	1.073 ±0.005	1.059 ±0.010	1.041 ±0.004	1.016 ±0.006	1.021 ±0.007
RMS, %	1.3±0.3	2.7±0.6	0.8±0.2	1.6±0.6	2.0±0.5

Table 20: The calibration constants (pC/GeV) for the extended barrel module EBM− (ANL-44) for η scan (TB-07-2002), the fit method.

η	10 GeV	20 GeV	180 GeV
−1.05	1.050	1.055	1.048
−1.15	1.034	1.035	1.023
−1.25	1.025	1.032	1.038
−1.35	1.089	1.093	1.077
−1.45		1.044	1.045
mean	1.050±0.014	1.052±0.011	1.048±0.009
RMS, %	2.8±1.0	2.5±0.8	2.0 ±0.6

Table 21: The calibration constants (pC/GeV) for the extended barrel EBM+ (IFA-42) for η scan (TB-07-2002), the fit method.

η	10 GeV	20 GeV	180 GeV
1.05	0.988	0.998	1.023
1.15	0.997	1.004	1.000
1.25	1.067	1.071	1.086
1.35	1.005	1.016	1.033
mean	1.014±0.018	1.022±0.017	1.035±0.018
RMS, %	3.6±1.3	3.3±1.2	3.7±1.3

Table 22: The calibration constants (pC/GeV) for the BM− (JINR-55) barrel module for η scan (TB-07-2002), the fit filter method. Accuracy of constants is 0.005.

η	10 GeV	20 GeV	50 GeV	100 GeV	180 GeV
−0.05	1.057	1.035	1.018	1.171	1.103
−0.15	1.051	1.039		1.051	1.162
−0.25	1.084	1.075	1.067	1.012	1.040
−0.35	1.068	1.068	1.050	1.034	1.055
−0.45	1.076	1.076	1.050	1.032	1.065
−0.55	1.072	1.080		1.065	1.096
−0.65	1.062	1.061		1.037	1.062
−0.75	1.052	1.051		0.981	1.010
−0.85	1.030	1.032		1.018	1.044
mean	1.061 ±0.005	1.057 ±0.006	1.046 ±0.010	1.031 ±0.022	1.071 ±0.015
RMS, %	1.6±0.4	1.9±0.4	2.0±0.7	6.6±1.5	4.4±1

Table 23: The calibration constants (pC/GeV) for the BM+ (JINR-55) barrel module for η scan (TB-07-2002), the fit filter method. Accuracy of constants is 0.005.

η	10 GeV	20 GeV	50 GeV	100 GeV	180 GeV
+0.05	1.010	1.004			
+0.15	1.056	1.045			
+0.25					0.986
+0.35	1.051	1.049			1.037
+0.45	1.076	1.072			1.079
mean	1.048 ±0.014	1.025 ±0.021			1.034 ±0.027
RMS, %	2.8±1	4.7±1.5			4.7±1.9

Table 24: The calibration constants (pC/GeV) for the EBM+ (IFA-42)$^{(*)}$ module tilerows at $\theta = 90^\circ$ (TB-07-2002), the fit method.

Tile	10 GeV	20 GeV	50 GeV	100 GeV	180 GeV
1	1.122	1.126			1.150
2	1.092	1.092	1.078	1.084	1.125
3	1.054	1.059			1.076
4	1.190	1.188			1.206
5	1.167	1.169	1.157	1.154	1.183
6	1.145	1.144			1.156
7	1.089	1.093			1.106
8	1.067	1.069			1.089
9	1.080	1.087			1.106
10	1.071	1.072		1.042	1.089
11	1.007	1.009			1.020
mean	1.098 ±0.016	1.101 ±0.016	1.118 ±0.04	1.093 ±0.033	1.118 ±0.016
RMS, %	5.3±1.1	5.8±1.1	5.6±2.8	5.6±2.3	5.3±1.1

$^{(*)}$ The electromagnetic calibration constants for tilerows 4 – 17 (cell B15) are systematically large than average for module IFA-42.

Table 25: The calibration constants (pC/GeV) for the EBM− (ANL-44) module tilerows at $\theta = 90°$ (TB-07-2002), the fit method.

Tile	10 GeV	20 GeV	50 GeV	100 GeV	180 GeV
1	1.023	1.024			1.041
2	1.118	1.125	1.103	1.110	1.151
3	1.040	1.048			1.067
4	1.045	1.049			
5	1.055	1.063	1.053	1.049	1.085
6	1.047	1.051			1.070
7	1.024	1.032			1.048
8	1.016	1.008			1.035
9	1.058	1.059			1.067
10	1.113	1.118	1.090	1.093	1.141
11	1.005	0.9981			1.007
mean	1.049 ±0.011	1.052 ±0.012	1.082 ±0.015	1.084 ±0.018	1.071 ±0.014
RMS, %	3.4±0.7	3.8±0.8	2.4±1.0	2.9±1.2	4.2±0.9

Table 26: The calibration constants (pC/GeV) for the BM− (JINR-55) barrel module tilerows at $\theta = 90°$ (TB-07-2002), the fit method.

Tile	10 GeV	20 GeV	50 GeV	100 GeV	180 GeV
1	1.087	0.9597			1.102
2	1.121	1.128	1.110	1.113	
3	1.094	1.108			1.120
4	1.093	1.098			1.096
5	1.077	1.085	1.067	1.065	1.082
6	1.108	1.114			1.103
7	1.146	1.088			1.083
8	1.149	1.146			1.140
9	1.084	1.085			1.080
10	1.057	1.025	1.026	1.029	1.082
11	1.046	1.026			1.078
mean	1.096 ±0.010	1.078 ±0.016	1.068 ±0.024	1.069 ±0.024	1.097 ±0.006
RMS, %	3.0±0.6	5.0±1.0	4.2±1.7	4.2±1.7	1.9±0.4

Table 27: The calibration constants (pC/GeV) for the BM+ (JINR-55) barrel module tilerows at $\theta = 90^\circ$ (TB-07-2002), the fit method.

Tile	10 GeV	20 GeV	50 GeV	100 GeV	180 GeV
1	1.111	1.111			
2	1.113	1.124	1.120	1.067	1.062
3	1.079	1.090			1.033
4	1.055	1.059			1.055
5	1.044	1.041	1.029	1.020	1.029
6	1.152	1.154			1.153
7	1.109	1.098			1.082
8	1.106	1.096			1.082
9	1.095	1.084			
10	1.034	1.017	1.002	1.010	1.041
11	1.099	1.069			1.090
mean	1.091 ±0.010	1.086 ±0.012	1.050 ±0.036	1.032 ±0.018	1.070 ±0.013
RMS, %	3.2±0.7	3.5±0.8	6.2±2.5	3.0±1.2	3.6±0.8

C.3.2 The Flat Filter Method results

Table 28: The calibration constants (pC/GeV) for the extended barrel modules at $\theta = 20^{\circ}$: EBM+ (IFA-42, A+12 ÷ A+16) and EBM+ (ANL-44, A−12 ÷ A−16), the flat filter method. Accuracy of constants is 0.005.

	High Gain		Low Gain		
Cell	10 GeV	20 GeV	50 GeV	100 GeV	180 GeV
A+12	1.159	1.161	1.193	1.176	1.191
A+13	1.144	1.146	1.151	1.161	1.179
A+14	1.140	1.146	1.173	1.154	1.180
A+15	1.133	1.137	1.158	1.138	
A+16	1.128	1.149	1.194	1.167	1.186
mean	1.141 ±0.005	1.148 ±0.004	1.174 ±0.009	1.159 ±0.006	1.184 ±0.03
mean	1.144±0.003		1.171±0.005		
RMS,%	1.1±0.4	0.9±0.3	2.0±0.6	1.4±0.4	0.6±0.2
RMS,%	1.0±0.2		1.7±0.3		
A−12	1.152	1.150	1.196	1.170	1.176
A−13	1.181	1.138	1.175	1.154	1.169
A−14	1.115	1.120		1.123	1.144
A−15	1.103	1.112	1.137	1.138	1.160
A−16	1.188	1.201	1.228	1.212	1.231
mean	1.148 ±0.012	1.144 ±0.016	1.184 ±0.019	1.159 ±0.015	1.176 ±0.015
mean	1.146±0.01		1.172±0.009		
RMS,%	3.8±1.2	3.5±1.1	3.8±1.3	3.4±1.1	3.3±1.0
RMS,%	3.4±0.8		3.4±0.6		

Table 29: The calibration constants (pC/GeV) for the JINR-55 barrel module at $\theta = 20°$. Accuracy of constants is 0.005, the flat filter method.

	High Gain		Low Gain		
Cell	10 GeV	20 GeV	50 GeV	100 GeV	180 GeV
A+1	1.122	1.112		1.146	1.128
A+2	1.137	1.160	1.145	1.152	1.143
A+3					
A+4	1.144	1.112		1.127	1.117
A+5	1.135	1.121	1.157	1.153	
A+6	1.138	1.128	1.177	1.168	
A+7	1.148	1.137	1.173	1.150	1.151
A+8	1.130	1.114	1.160	1.130	1.131
A+9	1.178	1.209			1.177
A+10	1.166	1.150	1.184	1.137	1.130
mean	1.144 ±0.006	1.138 ±0.010	1.166 ±0.006	1.145 ±0.005	1.140 ±0.007
mean	1.145±0.005		1.152±0.004		
RMS,%	1.5±0.4	2.8±0.6	1.2±0.4	1.2±0.3	2.0±0.5
RMS,%	1.0±0.4		1.8±0.3		
A−1	1.160	1.154	1.164	1.149	1.148
A−2	1.123	1.117	1.165	1.137	1.139
A−3	1.158	1.156	1.178	1.144	1.178
A−4	1.169	1.164	1.174	1.181	1.165
A−5	1.167	1.166	1.164	1.185	1.204
A−6	1.178	1.185	1.222	1.205	1.198
A−7	1.156	1.141	1.156	1.157	1.157
A−8	1.164	1.155	1.222	1.138	1.163
A−9	1.135	1.128	1.153	1.144	1.164
A−10	1.140	1.119	1.130		
mean	1.155 ±0.005	1.148 ±0.007	1.173 ±0.009	1.160 ±0.008	1.168 ±0.007
mean	1.152±0.004		1.167±0.005		
RMS,%	1.7±0.4	2.2±0.5	2.9±0.6	2.4±0.6	2.2±0.5
RMS,%	1.9±0.3		2.5±0.3		

Table 30: The calibration constants (pC/GeV) for the two extended barrel modules for various η: EBM+ (IFA-42) for $\eta > 0$ and EBM− (ANL-44) for $\eta < 0$, the flat filter method.

	High Gain		Low Gain
η	10 GeV	20 GeV	180 GeV
1.05	1.075	1.092	1.160
1.15	1.073	1.088	1.138
1.25	1.154	1.165	1.216
1.35	1.083	1.099	1.163
mean	1.096±0.020	1.111±0.018	1.169±0.016
mean	1.103± 0.010		1.169±0.016
RMS,%	3.9±1.4	3.6±1.3	3.3±1.2
RMS,%	3.6 ± 0.9		3.3±1.2
−1.05	1.130	1.140	1.181
−1.15	1.112	1.119	1.156
−1.25	1.107	1.120	1.173
−1.35	1.185	1.196	1.217
−1.45		1.129	1.181
mean	1.134±0.018	1.141±0.014	1.182±0.010
mean	1.138± 0.010		1.182±0.010
RMS,%	3.6±1.3	3.2±1	2.2 ±0.7
RMS,%	3.2 ± 0.7		2.2 ±0.7

Table 31: The calibration constants (pC/GeV) for the BM± (JINR-55) barrel module for η scan, the flat filter method. Accuracy of constants is 0.005.

	High Gain		Low Gain		
η	10 GeV	20 GeV	50 GeV	100 GeV	180 GeV
−0.05	1.138	1.125	1.084	1.314	1.104
−0.15	1.115	1.123	1.106	1.051	1.106
−0.25	1.164	1.164	1.186	1.129	1.161
−0.35	1.145	1.155	1.175	1.159	1.182
−0.45	1.136	1.146	1.178	1.158	1.195
−0.55	1.138	1.159	1.196	1.191	1.223
−0.65	1.123	1.133	1.168	1.162	1.190
−0.75	1.123	1.131	1.125	1.102	1.120
−0.85	1.111	1.121	1.150	1.145	1.172
mean	1.132 ±0.005	1.140 ±0.006	1.152 ±0.013	1.157 ±0.024	1.161 ±0.014
mean	1.136± 0.004		1.157± 0.010		
RMS,%	1.6±0.4	1.6±0.4	3.9±0.9	7.2±1.7	4.2±1
RMS,%	1.6 ± 0.3		5.1± 0.7		
+0.05	1.068	1.076			1.340
+0.15	1.107	1.115			1.107
+0.25					
+0.35	1.133	1.139			1.171
+0.45	1.133	1.138			1.207
mean	1.110 ±0.015	1.117 ±0.014			1.206 ±0.049
mean	1.113±0.010		1.206±0.049		
RMS,%	3.1±1.1	2.9±1.0			9.8±3.5
RMS,%	2.8± 0.7		9.8±3.5		

Table 32: The calibration constants (pC/GeV) for the extended barrel modules at $\theta = 90°$: EBM− (IFA-42, T+1 ÷ T+11) and EBM+ (ANL-44, T−1 ÷ T−11), the flat filter method.

	High Gain		Low Gain		
Tile	10 GeV	20 GeV	50 GeV	100 GeV	180 GeV
T+1	1.213	1.226			1.306
T+2	1.178	1.186	1.236	1.238	1.277
T+3	1.143	1.155			1.228
T+4	1.311	1.310			1.367
T+5	1.282	1.287	1.315	1.312	1.339
T+6	1.265	1.265			1.315
T+7	1.198	1.205			1.255
T+8	1.147	1.154			1.230
T+9	1.159	1.173			1.251
T+10	1.155	1.162	1.192	1.188	1.236
T+11	1.084	1.092			1.158
mean	1.194 ±0.021	1.201 ±0.020	1.248 ±0.036	1.246 ±0.036	1.267 ±0.018
mean	1.198± 0.014		1.261± 0.014		
RMS,%	6.8±1.5	6.5±1.4	6.2±2.5	6.2±2.5	5.9±1.3
RMS,%	6.5± 1.0		5.7± 1.0		
T−1		1.122			1.194
T−2	1.225	1.239	1.283	1.297	1.323
T−3	1.142	1.155			1.231
T−4	1.141	1.147			1.195
T−5	1.149	1.159	1.196	1.201	1.230
T−6	1.147	1.153			1.219
T−7	1.119	1.130			1.191
T−8	1.113	1.108			1.182
T−9	1.152	1.158			1.214
T−10	1.218	1.227	1.254	1.262	1.299
T−11	1.100	1.096			1.151
mean	1.151 ±0.013	1.154 ±0.013	1.244 ±0.026	1.253 ±0.028	1.219 ±0.015
mean	1.152± 0.009		1.231± 0.012		
RMS,%	3.6±0.8	3.8±0.8	3.6±1.4	3.8±1.6	4.1±0.9
RMS,%	4.2 ± 0.6		4.8± 0.8		

Table 33: The calibration constants (pC/GeV) for the BM± (JINR-55) barrel module at $\theta = 90°$, the flat filter method.

	High Gain		Low Gain		
tile	10 GeV	20 GeV	50 GeV	100 GeV	180 GeV
BM−1	1.171				1.232
BM−2	1.208	1.221	1.256	1.250	1.267
BM−3	1.183	1.204			1.256
BM−4	1.160	1.175			1.225
BM−5	1.142	1.157	1.212	1.199	1.208
BM−6	1.180	1.196			1.241
BM−7	1.219	1.171			1.218
BM−8	1.222	1.231			1.268
BM−9	1.159	1.170			1.216
BM−10	1.109	1.095	1.142	1.142	1.203
BM−11	1.099	1.099			1.201
mean	1.168 ±0.012	1.172 ±0.014	1.203 ±0.033	1.197 ±0.03	1.230 ±0.007
mean	1.170± 0.009		1.220± 0.009		
RMS,%	3.5±0.7	3.9±0.9	5.7±2.3	5.4±2.2	2.0±0.4
RMS,%	4.2± 0.6		3.7± 0.6		
BM+1	1.194	1.203			1.187
BM+2	1.192	1.213	1.265	1.201	1.190
BM+3	1.164	1.185			1.167
BM+4	1.125	1.136			1.186
BM+5	1.112	1.115	1.163	1.150	1.154
BM+6	1.230	1.240			1.293
BM+7	1.191	1.188			1.166
BM+8	1.187	1.188			1.214
BM+9	1.181	1.178			1.206
BM+10	1.108	1.114	1.141	1.139	1.170
BM+11	1.176	1.179		1.137	1.219
mean	1.169 ±0.012	1.176 ±0.012	1.190 ±0.038	1.163 ±0.019	1.196 ±0.012
mean	1.173± 0.008		1.189± 0.010		
RMS,%	3.3±0.7	3.4 ±0.7	6.6±2.7	3.3±1.4	3.2± 0.7
RMS,%	3.8± 0.6		4.2± 0.7		

C.3.3 The average calibration constants

Table 34: The average calibration constants and RMS (%) values of the A-cell scan at $\theta = 20°$, η scan and the tilerow scan at $\theta = 90°$ for ANL-44, IFA-42 and JINR-55 modules, the fit method (TB-07-2002) [13].

Module	20°		η		90°	
	R_e	RMS %	R_e	RMS %	R_e	RMS %
ANL-44	1.038±0.006	3.2±0.4	1.049±0.006	2.2±0.4	1.061±0.006	3.9±0.5
IFA-42	1.046±0.004	2.0±0.3	1.024±0.010	3.3±0.7	1.106±0.008	5.1±0.6
JINR-55−	1.051±0.004	3.2±0.3	1.054±0.006	4.1±0.5	1.087±0.006	3.9±0.4
JINR-55+	1.043±0.005	2.9±0.3	1.035±0.011	3.9±0.8	1.076±0.007	4.1±0.5
mean	1.046±0.002	3.0±0.2	1.046±0.004	3.8±0.3	1.082±0.004	4.5±0.3

Table 35: The average calibration constants and RMS (%) values for the A-cell scan at $\theta = 20°$, η scan and the tilerow scan at $\theta = 90°$, the flat filter method (TB-07-2002) [12].

Module	20°		η		90°	
	R_e pC/GeV	RMS %	R_e pC/GeV	RMS %	R_e pC/GeV	RMS %
ANL-44	1.161±0.007	3.6±0.5	1.153±0.009	3.5±0.7	1.187±0.010	5.9±0.7
IFA-42	1.160±0.004	2.0±0.3	1.126±0.013	4.6±0.9	1.225±0.011	6.9±0.8
JINR-55−	1.161±0.003	2.4±0.2	1.148±0.006	4.2±0.4	1.192±0.008	4.7±0.5
JINR-55+	1.147±0.004	2.0±0.2	1.127±0.012	4.0±0.8	1.180±0.006	4.0±0.5
mean	1.157±0.002	2.6±0.2	1.143±0.005	4.2±0.3	1.196±0.005	5.7±0.3

C.4 Test beam: 08-2002

Table 36: The calibration constants (pC/GeV) for the TileCal Extended Barrel Modules "ANL-27" and "IFA-09" at $\theta = 20°$ obtained using the flat filter method (TB-08-2002).

	20 GeV	180 GeV	20 GeV	180 GeV
Cell	EBM− (ANL-27)		EBM+ (IFA-09)	
12	1.161±0.002	1.193±0.002	1.158±0.002	1.179±0.002
13	1.153±0.002	1.181±0.002	1.115±0.002	1.140±0.002
14	1.147±0.002	1.171±0.002	1.115±0.002	1.159±0.002
15	1.157±0.002	1.170±0.002	1.134±0.002	1.153±0.002
16	1.177±0.002	1.194±0.002	1.081±0.002	1.066±0.002
mean	1.16 ± 0.01	1.18 ± 0.01	1.12 ± 0.01	1.14 ± 0.01

Table 37: The calibration constants (pC/GeV) for the TileCal Barrel Module "JINR-01" at $\theta = 20°$ obtained using the flat filter method (TB-08-2002) [14]. Accuracy of constants is 0.002.

	20 GeV	180 GeV	20 GeV	180 GeV
Cell	BM− (JINR-01)		BM+ (JINR-01)	
1	1.193	1.193	—	1.166
2	1.178	1.197	1.187	1.187
3	1.183	1.161	1.147	1.171
4	1.220	1.184	1.164	1.155
5	1.122	1.146	1.171	1.185
6	1.135	1.171	1.203	1.187
7	1.173	1.206	1.186	1.199
8	1.184	1.231	1.161	1.121
9	1.137	1.182	1.114	1.120
10	1.140	1.101	1.226	1.207
mean	1.17 ± 0.01	1.18 ± 0.01	1.17 ± 0.01	1.17 ± 0.01

Table 38: Calibration Constants (pC/GeV) for high and low gain for TileCal Modules ANL-27, IFA-09 and JINR-01 at 20° obtained using the flat filter method (TB-08-2002) [14].

		Calibration Constants (pC/GeV)	
TileCal Module		High Gain (20 GeV)	Low Gain (180 GeV)
ANL-27:	EBM−	1.16 ± 0.01	1.18 ± 0.01
IFA-09:	EBM+	1.12 ± 0.01	1.14 ± 0.01
JINR-01:	BM−	1.17 ± 0.01	1.18 ± 0.01
	BM+	1.17 ± 0.01	1.17 ± 0.01

Table 39: The calibration constants (pC/GeV) for the TileCal Extended Barrel Modules "ANL-27" and "IFA-09" at $\theta = 90°$ obtained using the flat filter method (TB-08-2002) [14].

	20 GeV	180 GeV	20 GeV	180 GeV
Tile	EBM− (ANL-27)		EBM+ (IFA-09)	
1	—	1.338±0.002	1.200±0.002	1.267±0.002
2	1.281±0.002	1.300±0.002	1.265±0.002	1.299±0.002
3	1.178±0.002	1.230±0.002	—	1.207±0.002
4	1.327±0.002	1.293±0.002	1.198±0.002	1.248±0.002
5	1.133±0.002	1.120±0.002	1.177±0.002	1.203±0.002
6	1.194±0.002	1.174±0.002	—	1.243±0.002
7	1.130±0.002	1.122±0.002	1.157±0.002	1.218±0.002
8	—	1.225±0.002	1.223±0.002	1.208±0.002
9	1.211±0.002	1.231±0.002	1.168±0.002	1.324±0.002
10	1.220±0.002	1.218±0.002	1.164±0.002	1.145±0.002
11	1.117±0.002	1.123±0.002	1.143±0.002	1.137±0.002
mean	1.19 ± 0.02	1.21 ± 0.02	1.19 ± 0.01	1.23 ± 0.02

Table 40: The calibration constants (pC/GeV) for the TileCal Barrel Module "JINR-01" at $\theta = 90°$ obtained using the flat filter method (TB-08-2002) [14].

	20 GeV	180 GeV	20 GeV	180 GeV
Tile	BM− (JINR-01)		BM+ (JINR-01)	
1	1.259±0.002	1.219±0.002	—	1.216±0.002
2	1.180±0.002	1.039±0.002	1.263±0.002	1.321±0.002
3	1.351±0.002	1.328±0.002	—	1.202±0.002
4	1.210±0.002	1.220±0.002	1.238±0.002	1.247±0.002
5	1.218±0.002	1.206±0.002	1.194±0.002	1.198±0.002
6	1.165±0.002	1.089±0.002	—	1.181±0.002
7	1.099±0.002	1.090±0.002	—	1.218±0.002
8	1.244±0.002	1.233±0.002	1.210±0.002	1.224±0.002
9	1.155±0.002	1.143±0.002	1.120±0.002	1.088±0.002
10	1.222±0.002	1.209±0.002	1.202±0.002	1.195±0.002
11	1.112±0.002	1.108±0.002	1.182±0.002	1.176±0.002
mean	1.19 ± 0.02	1.16 ± 0.02	1.20 ± 0.02	1.21 ± 0.02

Table 41: The average calibration constants (pC/GeV) for low and high gains at 90° obtained using the flat filter method (TB-08-2002) [14].

		Calibration Constants (pC/GeV)	
TileCal Module		High Gain (20 GeV)	Low Gain (180 GeV)
ANL-27:	EBM−	1.19 ± 0.02	1.21 ± 0.02
IFA-09:	EBM+	1.19 ± 0.01	1.23 ± 0.02
JINR-01:	BM−	1.19 ± 0.02	1.16 ± 0.02
	BM+	1.20 ± 0.02	1.21 ± 0.02

C.5 Test beam: 06-2003

Table 42: The calibration constants (pC/GeV) for the extended barrel modules ANL-03 and ANL-23 for 180 GeV at $\theta = 20^\circ$ (TB-06-2003).

	flat	fit	flat	fit
Cell	EBM− (ANL-23)		EBM+ (ANL-03)$^{(*)}$	
12	1.130±0.002	1.003±0.0008	1.137±0.002	1.039±0.001
13	1.093±0.001	1.003±0.0006	1.057±0.001	.9462±0.001
14	1.111±0.001	.9813±0.0007	1.103±0.002	.9840±0.001
15	1.118±0.002	1.018±0.0007	1.085±0.001	.9962±0.001
16	1.143±0.002	1.032±0.0006	1.034±0.001	.9134±0.001

$^{(*)}$ We did not use these ANL-03 data in the analysis because the these calibration constants are systematically small.

Table 43: The calibration constants (pC/GeV) for the TileCal Barrel Module "JINR-12" at $\theta = 20^\circ$ obtained using the flat and fit methods (TB-06-2003) [14].

	flat	fit	flat	fit
Cell	BM− (JINR-12)		BM+ (JINR-12)	
1	1.063±0.009	0.995±0.001	1.102±0.003	1.001±0.002
2	1.126±0.004	1.022±0.001	1.172±0.001	1.033±0.002
3	1.159±0.002	1.041±0.002	1.134±0.002	0.992±0.002
4	1.120±0.002	0.997±0.002	1.205±0.003	1.039±0.002
5	1.151±0.002	1.044±0.001	1.105±0.002	0.999±0.002
6	1.152±0.004	1.048±0.0009	1.208±0.0002	1.062±0.002
7	1.160±0.0006	1.046±0.001	1.170±0.001	1.064±0.002
8	1.152±0.002	1.022±0.0008	1.146±0.002	1.025±0.0008
9	1.111±0.0006	1.024±0.0004	1.151±0.003	1.038±0.002
10	1.081±0.003	0.959±0.0009		

Table 44: The calibration constants (pC/GeV) for the extended barrel modules ANL-03 and ANL-23 for 180 GeV at $\theta = 90°$ (TB-06-2003)

	flat	fit	flat	fit
Tile	EBM− (ANL-23)		EBM+ (ANL-03)	
1	1.142±0.002	1.029±0.002	1.145±0.002	1.007±0.0013
2	1.253±0.001	1.128±0.001	1.223±0.001	1.076±0.0009
3	1.138±0.001	1.018±0.001	1.289±0.001	1.135±0.0012
4	1.244±0.001	1.126±0.001	1.262±0.002	1.128±0.0015
5	1.184±0.001	1.071±0.001	1.173±0.002	1.052±0.0012
6	1.191±0.001	1.071±0.001	1.170±0.002	1.047±0.0006
7	1.074±0.002	0.962±0.001	1.157±0.002	1.033±0.001
8	1.204±0.002	1.069±0.001		1.040±0.001
9	1.083±0.001	0.952±0.001	1.209±0.001	1.057±0.001
10	1.303±0.002	1.159±0.001	1.225±0.002	1.066±0.001
11	1.175±0.001	1.045±0.001	1.091±0.002	0.952±0.001

Table 45: The calibration constants (pC/GeV) for the TileCal Barrel Module "JINR-12" at $\theta = 90°$ obtained using the flat and fit methods (TB-06-2003) [14].

	flat	fit	flat	fit
Tile	BM− (JINR-12)		BM+ (JINR-12)	
1	1.223±0.001	1.079±0.001	1.275±0.002	1.151±0.001
2	1.242±0.001	1.101±0.001		
3	1.174±0.001	1.034±0.001	1.189±0.001	1.074±0.001
4	1.197±0.002	1.058±0.001	1.199±0.002	1.081±0.001
5	1.222±0.002	1.084±0.001	1.220±0.002	1.101±0.001
6	1.154±0.001	1.018±0.001	1.169±0.002	1.057±0.001
7	1.162±0.001	1.064±0.001	1.145±0.002	1.028±0.001
8	1.048±0.001	0.954±0.001	1.200±0.002	1.075±0.001
9	1.125±0.001	1.020±0.001	1.146±0.003	1.029±0.001
10	1.174±0.001	1.046±0.001	1.123±0.001	1.015±0.001
11			1.143±0.001	1.018±0.001

Table 46: The average calibration constants (pC/GeV) for the ANL-23, ANL-03, JINR-12 modules (TB-06-2003) at 180 GeV for $\theta = 20°$ (cell-scan) [15]

TileCal Module		flat	fit	$\frac{flat}{fit}$
ANL-23:	$EBM-$	1.118 ± 0.020	1.008 ± 0.018	1.11 ± 0.03
ANL-03:	$EBM+$	1.083 ± 0.020	0.979 ± 0.018	1.11 ± 0.03
JINR-12:	$BM-$	1.128 ± 0.014	1.019 ± 0.013	1.11 ± 0.02
	$BM+$	1.156 ± 0.015	1.028 ± 0.013	1.12 ± 0.02

Table 47: The average calibration constants (pC/GeV) for the ANL-23, ANL-03, JINR-12 modules (TB-06-2003) at 180 GeV for $\theta = 90°$ (tile-scan) [15]

TileCal Module		flat	fit	flat/fit
ANL-23:	$EBM-$	1.173 ± 0.014	1.053 ± 0.013	1.11 ± 0.02
ANL-03:	$EBM+$	1.196 ± 0.015	1.057 ± 0.013	1.13 ± 0.02
JINR-12:	$BM-$	1.167 ± 0.015	1.039 ± 0.013	1.12 ± 0.02
	$BM+$	1.183 ± 0.015	1.066 ± 0.013	1.11 ± 0.02

C.6 Test beam: 07-1-2003

Table 48: The calibration constants (pC/GeV) for the EBM+ (ANL-30) and EBM− (IFA-27) (TB-07-1-2003) at 100 GeV and 180 GeV and $\theta = 20^\circ$ for flat filter and fit methods. Accuracy of constants is 0.004 [17].

	flat	flat	fit	fit
Cell	100 GeV	180 GeV$^{(*)}$	100 GeV	180 GeV
A+12	1.146	1.026		
A+13	1.110			
A+14	1.132	1.053		
A+15	1.161	1.180	1.007	1.040
A+16	1.160	1.004		
A−15	1.1	1.137	1.024	1.008
A−16	1.1	1.143	1.024	1.008

$^{(*)}$ We did not use these results for ANL-30 in analysis because the calibration constants are systematically small.

Table 49: The calibration constants (pC/GeV) for the BM+ and BM− (JINR-27) at $\theta = 20^\circ$ (TB-07-1-2003), the flat filter method. Accuracy of constants is 0.004. [17].

Cell	100 GeV	180 GeV	Cell	100 GeV	180 GeV
A+1	1.155	1.148	A−1	1.150	1.147
A+2			A−2	1.145	1.138
A+3		1.178	A−3	1.188	1.174
A+4	1.148	1.134	A−4	1.134	1.123
A+5	1.141	1.129	A−5	1.180	1.170
A+6	1.158	1.148	A−6	1.149	1.145
A+7	1.176	1.154	A−7	1.148	1.147
A+8	1.152	1.123	A−8	1.166	1.158
A+9	1.166	1.166	A−9	1.167	1.150
A+10			A−10	1.135	1.116

Table 50: The electromagnetic calibration constants (pC/GeV) for the BM+ and BM− (JINR-27) at $\theta = 20^\circ$ (TB-07-1-2003), the fit method. Accuracy of constants is 0.004 [17].

Cell	100 GeV	180 GeV	Cell	100 GeV	180 GeV
A+1	1.030	1.026	A−1	1.026	1.024
A+2			A−2	1.025	1.019
A+3		1.053	A−3	1.057	1.045
A+4	1.030	1.007	A−4	1.009	1.100
A+5	1.012	1.004	A−5	1.056	1.049
A+6	1.034	1.027	A−6	1.036	1.030
A+7	1.049	1.030	A−7	1.026	1.024
A+8	1.030	1.005	A−8	1.040	1.036
A+9	1.040	1.104	A−9	1.039	1.026
A+10			A−10	1.006	0.990

Table 51: The average calibration constants for the BM+ and BM− (JINR-27) (TB-07-1-2003) at 100 GeV and 180 GeV and 20° using the flat filter and fit methods [17].

Module			100 GeV	180 GeV
BM−, JINR-27	flat	mean	1.156 ± 0.006	1.147 ± 0.006
		RMS,%	1.6 ± 0.4	1.6 ± 0.4
BM−, JINR-27	fit	mean	1.032 ± 0.005	1.024 ± 0.006
		RMS,%	1.7 ± 0.4	1.7 ± 0.4
BM+, JINR-27	flat	mean	1.157 ± 0.004	1.148 ± 0.007
		RMS, %	1.0 ± 0.3	1.6 ± 0.4
BM+, JINR-27	fit	mean	1.032 ± 0.004	1.024 ± 0.006
		RMS,%	1.1 ± 0.3	1.7 ± 0.4

Table 52: The average calibration constants for the EBM+ (ANL-30) and EBM− (IFA-27) (TB-07-1-2003) at 100 GeV and 180 GeV and 20° using the flat filter and fit methods. [17].

Module			100 GeV	180 GeV
EBM−, IFA-27	flat	mean	1.132 ± 0.005	1.140 ± 0.003
		RMS, %	1.4 ± 0.2	1.16 ± 0.01
EBM−, IFA-27	fit	mean	0.996 ± 0.005	1.008 ± 0.004
		RMS, %		
EBM+, ANL-30	flat	mean	1.14 ± 0.01	1.180 ± 0.004
		RMS, %	1.9 ± 0.7	
EBM+, ANL-30	fit	mean	1.006 ± 0.007	1.040 ± 0.004
		RMS, %	1.6 ± 0.5	

Table 53: The calibration constants (pC/GeV) for the TileCal Extended Barrel Modules EBM+ (ANL-30) and EBM− (IFA-27) at $\theta = 90°$ obtained using the flat filter method (TB-07-1-2003) [16]. Accuracy of constants is 0.002.

	100 GeV	180 GeV	350 GeV	100 GeV	180 GeV
Tile	EBM− (IFA-27)			EBM+ (ANL-30)	
1		1.130			1.220
2	1.217	1.219	1.147	1.146	1.186
3		1.150			1.146
4		1.197			1.226
5	1.188	1.181	1.108	1.231	1.221
6		1.190			1.193
7		1.098			1.157
8		1.149			1.182
9	1.279	1.286	1.207		1.218
10	1.176	1.132	1.106	1.157	1.152
11		1.143			1.100
mean	1.21 ±0.02	1.17 ±0.01	1.14 ±0.02	1.18 ±0.03	1.18 ±0.01

Table 54: The calibration constants (pC/GeV) for the TileCal Extended Barrel Modules EBM+ (ANL-30) and EBM− (IFA-27) at $\theta = 90°$ obtained using the fit method (TB-07-1-2003) [16]. Accuracy of constants is 0.002.

	100 GeV	180 GeV	350 GeV	100 GeV	180 GeV
Tile	EBM− (IFA-27)			EBM+ (ANL-30)	
1		1.071			1.043
2	1.067	1.077	1.058	1.004	1.008
3		1.011			1.080
4		1.067			1.080
5	1.042	1.051	1.011	1.085	1.049
6		1.056			1.014
7		0.977			1.057
8		1.028			1.088
9	1.137	1.145	1.109		1.014
10	0.989	0.999	0.960	1.005	0.980
11		1.012			0.992
mean	1.05 ±0.03	1.03 ±0.01	1.03 ±0.03	1.03 ±0.02	1.05 ±0.01

Table 55: The calibration constants (pC/GeV) for the TileCal Barrel Modules BM± (JINR-27) at $\theta = 90°$ obtained using the flat filter method (TB-07-1-2003) [16]. Accuracy of constants is 0.002.

	100 GeV	180 GeV	100 GeV	180 GeV
Tile	BM− (JINR-27)		BM+ (JINR-27)	
1		1.189		1.179
2	1.253	1.245	1.163	1.165
3		1.197		1.177
4		1.200		1.217
5	1.194	1.180	1.212	1.201
6		1.121		1.156
7		1.107		1.179
8		1.187		1.143
9	1.207	1.101	1.139	1.202
10	1.192	1.154	1.222	1.222
11		1.135		1.218
mean	1.21 ±0.02	1.16 ±0.01	1.18 ±0.02	1.19 ±0.01

Table 56: The calibration constants (pC/GeV) for the TileCal Barrel Modules BM± (JINR-27) at $\theta = 90^\circ$ obtained using the fit filter method (TB-07-1-2003) [16]. Accuracy of constants is 0.002.

	100 GeV	180 GeV	100 GeV	180 GeV
Tile	BM− (JINR-27)		BM+ (JINR-27)	
1		1.063		1.059
2	1.107	1.114	1.040	1.046
3		1.074		1.056
4		1.077		1.093
5	1.057	1.050	1.084	1.082
6		0.998		1.037
7		0.988		1.048
8		1.065		1.024
9	1.079	0.977	1.005	1.066
10	1.043	1.034	1.091	1.091
11		1.021		1.092
mean	1.07 ±0.02	1.04 ±0.01	1.05 ±0.02	1.06 ±0.01

Table 57: The average calibration constants for the EBM+ (ANL-30), EBM− (IFA-27), BM+ and BM− (JINR-27) at 100 GeV, 180 GeV and 350 GeV at 90° obtained with the flat filter method (TB-07-1-2003).

		Calibration Constants (pC/GeV)		
Module		100 GeV	180 GeV	350 GeV
IFA-27:	EBM−	1.21 ± 0.02	1.17 ± 0.01	1.14 ± 0.02
ANL-30:	EBM+	1.18 ± 0.03	1.18 ± 0.01	
JINR-27:	BM−	1.21 ± 0.02	1.16 ± 0.01	
	BM+	1.18 ± 0.02	1.19 ± 0.01	
Module-0:	BM0−	1.19 ± 0.04	1.14 ± 0.02	
	BM0+	1.22 ± 0.03	1.21 ± 0.02	

Table 58: The average calibration constants for the EBM+ (ANL-30), EBM− (IFA-27), BM+ and BM− (JINR-27) at 100 GeV, 180 GeV and 350 GeV at 90° obtained with the fit method (TB-07-1-2003).

		Calibration Constants (pC/GeV)		
TileCal Module		100 GeV	180 GeV	350 GeV
IFA-27:	EBM−	1.05 ± 0.03	1.03 ± 0.01	1.03 ± 0.03
ANL-30:	EBM+	1.03 ± 0.02	1.05 ± 0.01	
JINR-27:	BM−	1.07 ± 0.02	1.04 ± 0.01	
	BM+	1.05 ± 0.02	1.06 ± 0.01	
Module-0:	BM0−	1.07 ± 0.03	1.03 ± 0.02	
	BM0+	1.10 ± 0.03	1.10 ± 0.02	

D Modules Correspondence

Table 59: The correspondence between production ANL, IFA, JINR modules number and position of these modules in the assembled TileCal.

Long Barrel			Extended Barrel			
	A	C	A		C	
JINR01	LBA33	LBC33	ANL03	EBA13	IFA09	EBC30
JINR12	LBA01	LBC01	ANL08	EBA10	IFA15	EBC33
JINR13	LBA14	LBC14	ANL15	EBA07	IFA24	EBC49
JINR18	LBA49	LBC49	ANL23	EBA04	IFA27	EBC25
JINR27	LBA25	LBC25	ANL27	EBA47	IFA38	EBC64
JINR34	LBA58	LBC58	ANL30	EBA16	IFA42	EBC48
JINR54	LBA09	LBC09	ANL36	EBA44	IFA46	EBC19
JINR55	LBA31	LBC31	ANL44	EBA33	IFA59	EBC62
JINR63	LBA17	LBC17				